Research Activities

– Synchrotron Radiation Experiments –

Electron structure of $YbCu_{1-x}Al_x$ studied by low-energy photoemission spectroscopy

A. Kano[a], R. Kamimori[a], T. Matsumoto[a], M. Arita[b], N. Tsujii[c], H. Sato[b]

[a]*Graduate School of Advanced Science and Engineering, Hiroshima University, Higashi-Hiroshima 739-8526, Japan*
[b]*Hiroshima Synchrotron Radiation Center, Hiroshima University, Higashi-Hiroshima 739-0046, Japan*
[c]*International Center for Materials Nanoarchitectonics, National Institute for Materials Science, Tsukuba 305-0047, Japan*

Keywords: Kondo peak, quantum critical point, low-energy photoemission spectroscopy

The Yb-based compounds have been attracted interests because of its rich variety of intriguing physical properties derived from the localized Yb 4*f* states hybridized with conduction electrons (*c*-*f* hybridization). These phenomena are qualitatively discussed based on the so-called Doniach phase diagram. When the *c*-*f* hybridization is weak, RKKY interaction becomes dominant and the magnetic-order is realized at low temperature. In contrast, when the *c*-*f* hybridization is weak, the Kondo effect becomes dominant and the 4*f* moments are screened with the conduction electrons, leading to a non-magnetic Fermi liquid state. A boundary point at zero temperature separating the magnetic and non-magnetic ground state regions defines a quantum critical point (QCP). The unconventional physical properties such as a non-Fermi liquid state and a heavy-fermion superconductivity are discovered near QCP. In the study of 4*f* electron systems, one of the most important issues is to establish the electronic structure around QCP.

The $CaCu_5$-type hexagonal $YbCu_{5-x}Al_x$ is a suitable system to investigate how the electronic structure change from the non-magnetic Fermi liquid state to magnetic ordering state. The maximal temperature T_{max} of the magnetic susceptibility $YbCu_5$ is T_{max}~1000 K [1, 2]. With increasing the Al concentration (x), T_{max} is rapidly reduced and becomes close to zero K at x=1.5. Above x=1.5, the antiferromagnetic order appears below the Néel temperature of $T_N < 2$ K. The $YbCu_{1-x}Al_x$ system is expected to have QCP near x=1.5, where the system exhibits non-Fermi-liquid behavior [3]. In case of Yb compounds, so called Kondo singlet is observed in the low-energy photoemission spectra (LEPES spectra) as a peak near the Fermi level (E_F) at k_BT_K [4], where T_K stands for the Kondo temperature. Here, we report the LEPES spectra of $YbCu_{1-x}Al_x$ measured at undulator beamline BL-9A. Clean surfaces of the samples were prepared by fracturing *in situ*.

Figure 1 (a) shows the LEPES spectra near E_F of $YbCu_{5-x}Al_x$ (x=0, 0.6, 1.0, 1.25, 1.5, 1.75, 2.0) measured at 15 K. The excitation energy is $h\nu$=14 eV. LEPES spectrum of $YbCu_5$ (x=0) exhibits a broad peak around 0.24 eV, which is attributed to the Kondo peak [5]. The Kondo peak is shifted to E_F with increasing x, reflecting the decrease of T_K [2]. It is noted that the Kondo peak is observed in the LEPES spectrum of x=2.0, which suggests that the *c*-*f* hybridization is still remaining in the magnetic region above x>1.5. The peak energies are plotted as a function of x in Fig. 1 (b). The peak energy rapidly decreases from 0.24 eV at x=0 to 0.06 eV at x=1.0, and gradually decreases to 0.03 at x=0. The x-dependence of the peak energies is similar to that of T_K [2].

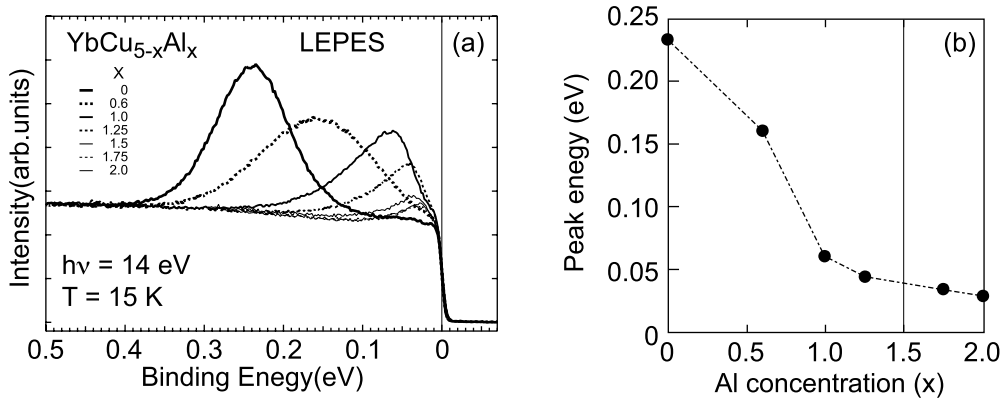

Fig. 1. (a) LEPES spectra near E_F of $YbCu_{5-x}Al_x$ measured at $h\nu$=14 eV and 15 K. (b) Energy positions of the Kondo peaks of $YbCu_{5-x}Al_x$ as a function of the Al concentration x.

REFERENCES

1. K. Yoshimura, N. Tsujii, J. He and K. Kosuge, JJAP Ser. **8**, 363 (1999).
2. H. Yamaoka, I. Jarrige, N. Tsujii, N. Hiraoka, H. Ishii and K.-D. Tsuei, Phys. Rev. B **80**, 035120 (2009).
3. E. Bauer, R. Hauser, A. Galatanu, H. Michor, G. Hilscher, J. Sereni, M. G. Berisso, P. Pedrazzini, M. Galli, F. Marabelli and P. Bonville, Phys. Rev. B **60**, 1238 (1999).
4. I. R. Blyth, J. J. Joyce, A. J. Arko, P. C. Canfield, A. B. Andrews, Z. Fisk, J. D. Thompson, R. J. Bartlett, P. Riseborough, J. Tang and J. M. Lawrence, Phys. Rev. B **48**, 9497 (1993).
5. K. Yoshikawa, H. Sato, M. Arita, Y. Takeda, K. Hiraoka, K. Kojima, K. Tsuji, H. Namatame and M. Taniguchi, Phys. Rev. B **72**, 165106 (2005).

Elucidation of the electronic state of halogen-bridged metal complexes by angle-resolved photoelectron spectroscopy

Masanori Wakizaka[a], Shiv Kumar[b], and Kenya Shimada[b]

[a] *Department of Chemistry, Graduate School of Science Tohoku University 6-3 Aramaki-Aza-Aoba, Aoba-Ku, Sendai 980-8578, Japan*
[b] *Hiroshima Synchrotron Radiation Center, Hiroshima University, 2-313 Kagamiyama, Higashi-Hiroshima 739-0046, Japan*

Keywords: Halogen-bridged metal complexes, One-dimensional electronic system, Nickel, Bromide

Halogen-bridged metal complexes (MX-Chains) are a sort of chain compounds (Figure 1a,b) [1]. Alternating metal ions and halides are bound using d_z^2 orbitals and p_z orbitals, which makes a one-dimensional (1D) electronic system. Ni type MX-Chins uniquely adopt a Mott-Hubbard (MH) state, i.e. an averaged-valence Ni(III) state, based on strong electron correlation. On the other hand, Pd type MX-Chains usually adopt a charge-density-wave (CDW) state, i.e., a mixed-valence Pd(II)/Pd(IV) state, because the electro-phono interaction energy is larger than the electron-electron repulsion energy. Recently, the heterostructure of $[Ni(chxn)_2Br]Br_2$ and $[Pd(chxn)_2Br]Br_2$ (chxn: 1*R*,2*R*-diaminocyclohexane) was synthesized [2]. Scanning tunneling microscope revealed that these two kinds of chains are connected at atomic-scale, which can be considered as a 1D heterojunction. Angle-resolved photoemission spectroscopy (ARPES) can be a powerful tool to reveal electronic state of such 1D material [3].

A single crystal of $[Ni(chxn)_2Br]Br_2$ was used as a sample for ARPES. Exposing X-ray beam, it did not show sufficient photoelectron intensity at the initial position. After adjustment of angle of the sample stage that the chain direction aligns to the X-ray direction (Figure 1c), intensity became larger. This phenomena is considered to relate with 1D electronic system of the MX-Chains. However, photoelectron intensity immediately decreased, suggesting decomposition of the chain. A softer method such as UVPES would be better.

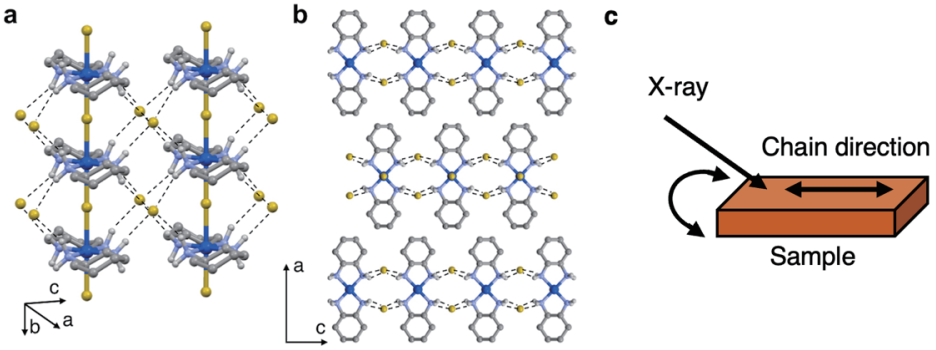

FIGURE 1. (a) Chain structure, (b) layer structure, and (c) an illustration of ARPES experiment of $[Ni(chxn)_2Br]Br_2$.

REFERENCES

1. M. Yamashita, *Bull. Chem. Soc. Jpn.* **94**, 209-264 (2021).
2. M. Wakizaka, S. Kumagai, H. Wu, T. Sonobe, H. Iguchi, T. Yoshida, M. Yamashita, S. Takaishi, *Nat. Commun*. **13**, 1188 (2022).
3. S. Fujimori, A. Ino, T. Okane, A. Fujimori, K. Okada, T. Manabe, M. Yamashita, H. Kishida, H. Okamoto, *Phys. Rev. Lett.* **88**, 247601 (2002).

Observation of electron structure of chiral magnet $Yb(Ni_{1-x}Cu_x)_3Al_9$ by ARPES

Y. Tanimoto[a], M. Sugimoto[b], R. Kamimori[a], H. Sato[c], M. Arita[c], S. Kumar[c], K. Shimada[c], S. Nakamura[d], S. Ohara[d]

[a]*Graduate School of Advanced Science and Engineering, Hiroshima University, Higashi-Hiroshima 739-8526, Japan*
[b]*Faculty of Science, Hiroshima University, Higashi-Hiroshima 739-8526, Japan*
[c]*Hiroshima Synchrotron Radiation Center, Hiroshima University, Higashi-Hiroshima 739-0046, Japan*
[d]*Graduate School of Engineering, Nagoya Institute of Technology, Nagoya 466-8555, Japan*

Keywords: chiral magnetic crystal, helical magnetism, angle resolved photoemission spectroscopy

Trigonal $YbNi_3Al_9$ has a chiral crystal structure belonging to space group of *R*32 (No. 155) and is of interest as the first chiral magnetic alloy discovered in 4*f* electron compounds [1]. The localized Yb 4*f* spins are magnetically ordered below *T*=3.4 K, ferromagnetic in the *ab*-plane, and exhibit left-handed or right-handed helical magnetism with period q_z=0.8 in the *c*-axis direction [2]. Substitution of Ni with Cu significantly alters the magnetic interaction and shortens the helical period to q_z=0.4 for $Yb(Ni_{0.94}Cu_{0.06})_3Al_9$. Spin-polarized conduction electrons are thought to be responsible for this phenomenon. In this study, angle-resolved photoemission spectroscopy (ARPES) was performed on $YbNi_3Al_9$ and $Yb(Ni_{0.94}Cu_{0.06})_3Al_9$ to investigate the band structure of conduction electron bands near the Fermi level (E_F). Single crystals used for the ARPES measurements were synthesized by the flux-method [3]. The experiments were performed at BL-1 and BL-9A of Hiroshima Synchrotron Radiation Center (HSRC), Hiroshima University.

Figures 1(a) and (b) show the ARPES intensity plots of $YbNi_3Al_9$ measured at *hv*=24 eV with *p*-polarized geometry along the $\bar{\Gamma}$-$\bar{M}$ and $\bar{\Gamma}$-$\bar{K}$ directions of the surface Brillouin zone, respectively. Some hole-like bands around the $\bar{\Gamma}$ point and an electron-like band around the $\bar{M}$ point cross E_F. The bands located at around E_B=2.0~3.0 eV are due to the Ni 3*d* states. A parabolic band with a top of E_B~3.0 eV centered at the $\bar{\Gamma}$ point is also observed.

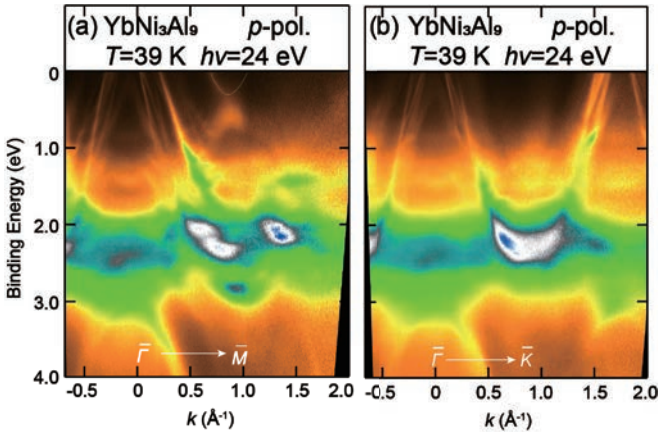

Fig. 1. ARPES intensity plots of $YbNi_3Al_9$ measured along (a) $\bar{\Gamma}$-$\bar{M}$ and (b) $\bar{\Gamma}$-$\bar{K}$ directions measured at *hv*=24 eV with *p*-polarized geometry.

Figures 2(a) and (b) represent the Fermi surfaces of $YbNi_3Al_9$ measured at *hv*=24 eV with *p*- and *s*-polarized geometries. The horizontal and vertical axes are the wavenumbers (k_x, k_y) along $\bar{\Gamma}$-$\bar{K}$ and $\bar{\Gamma}$-$\bar{M}$ directions, respectively. In Fig. 2(a), five hole-like Fermi surfaces, (a)~(e), were observed around the $\bar{\Gamma}$

point. The bands (b)~(e) in Fig. 2 (a) correspond to the bands (b')~(e') in Fig. 2 (b). The band (b) appears three-fold symmetric, reflecting the trigonal crystal structure with the three-fold symmetry. On the other hand, the (f) band at k_x=0.6~0.9 Å^{-1} and k_y=0.3~0.6 Å^{-1} in Fig. 2(a), which is not detected in Fig. 2(b), is an electronic-like Fermi surface. The (f) band has six-fold symmetry.

The Fermi surfaces of $Yb(Ni_{0.94}Cu_{0.06})_3Al_9$ becomes smaller in comparison with that of $YbNi_3Al_9$, although the feature is almost unchanged. This observation indicates the electron doping due to the substitution of Ni ion with Cu. The spin-resolved ARPES measurements for $YbNi_3Al_9$ are in progress.

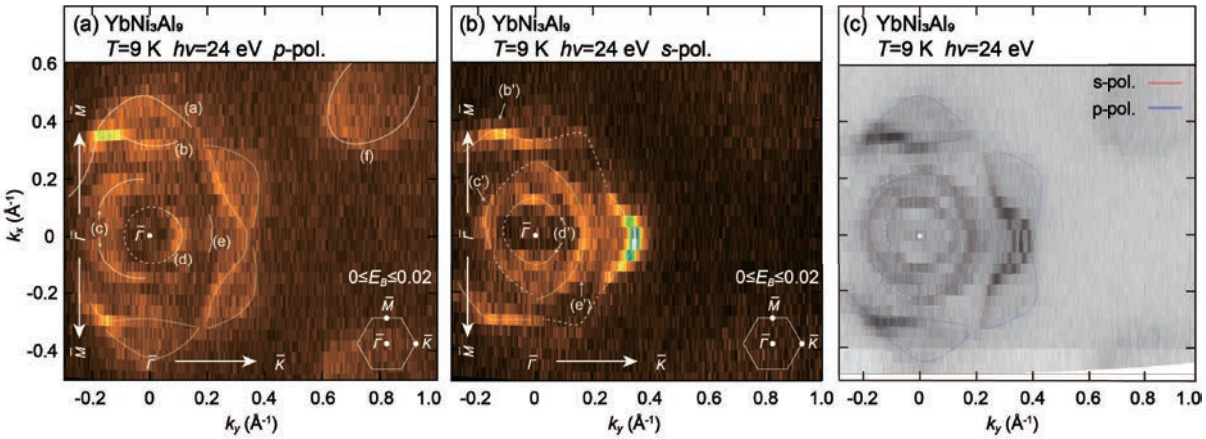

Fig. 2. Fermi surfaces of $YbNi_3Al_9$ measured at $h\nu$=24 eV with (a) *p*- and (b) *s*-polarized geometries.

REFERENCES

1. S. Ohara, S. Fukuta, K. Ohta, H. Kono, T. Yamashita, Y. Matsumoto and J. Yamaura, JPS Conf. Proc. **3**, 017016 (2014).
2. T. Matsumura, Y. Kita, K. Kubo, Y. Yoshikawa, S. Michimura, T. Inami, Y. Kousaka, K. Inoue and S. Ohara, J. Phys. Soc. Jpn. **86**, 124702 (2017).
3. T. Yamashita, R. Miyazaki, Y. Aoki and S. Ohara, J. Phys. Soc. Jpn. **81**, 034705 (2012).

The electronic structure investigation of dimensionality driven iridates

Takashi Komesu[a], Shiv Kumar[b], Armit Jadaun[b], Yuudai Miyai[b], Kenya Shimada[b], Yuanyuan Zhang[a], Xia Hong[a] and P. A. Dowben[a]

[a]*Department of Physics and Astronomy, Theodore Jorgensen Hall, 855 N 16th, University of Nebraska, Lincoln, NE 68588-0299, U.S.A.*
[b]*Hiroshima Synchrotron Radiation Center, Hiroshima University, Higashi-Hiroshima 739-0046, Japan*

Keywords: High Resolution Angle Resolved Photoemission Spectroscopy, Electronic Structure, spin-orbit interaction.

The 5d iridates (iridium oxides) exhibit some remarkable properties, most especially Mott physics, driven by electron correlation [1]. The Ruddlesden–Popper series iridates $Sr_{n+1}Ir_nO_{3n+1}$ show different properties depending on the value of n, which is a complication common to many complex oxides. Moon *et al.* [2] used optical spectroscopy and first-principles calculations to study the electronic structures of the 5*d* Ruddlesden–Popper series, there are some experimental band structures studies of $Sr_3Ir_2O_7$ (n = 2) single crystals, using ARPES [3,4]. It is clear that for many iridates [1], including $SrIrO_3$(001) [1,5], the band structure can change in the thin film limit. The obvious route forward is to perform film thickness dependent angle-resolved photoemission which could help elucidate the film thickness dependent behavior of the iridates [1,5-7].

Fig. 1 shows ARPES results from a 12.6 nm thick thin film $Sr_3Ir_2O_7$(001) single crystal, taken at HiSOR BL-1. Fig. 1 a) is for k_y direction and c) is for k_x direction, of surface parallel component. The surface Brillouin zone can be assigned from the extensive from low energy electron diffraction (LEED) studies as shown in Fig. 1. This is not the Brillouin zone proposed for $Sr_3Ir_2O_7$ (n = 2) single crystals, using ARPES [3,4], but rather a larger Brillouin zone with a smaller structural unity suggesting that some distortions of the perovskite lattice are insufficient to perturb the Brillouin zone and the band structure in the thin film limit.

The band dispersion for $Sr_3Ir_2O_7$(001) is quite similar to the one from previous results of $SrIrO_3$(001) thin film, as seen on Fig. 2. From the valance band structure of $SrIrO_3$(001) and $Sr_3Ir_2O_7$(001), in the vicinity of the Fermi level E_F, it appears that the density of states at near E_F is lower for $Sr_3Ir_2O_7$(001) compared to the $SrIrO_3$(001) thin films. To some extent, these results depend on iridate thickness not just because of the establish film thickness dependent metallicity seen for many iridates [1], but because the band structure is better defined with the thicker iridate films, as seen in Fig. 2,

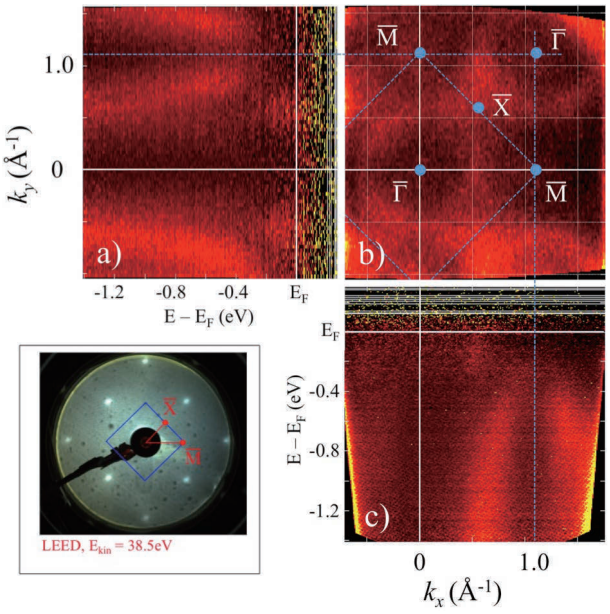

Fig. 1. The experimental valence band electronic structure of a 12.6 nm thick $Sr_3Ir_2O_7$(001) thin film as derived from angle-resolved photoemission, taken at room temperature with a photon energy of 71 eV. a) is the tilt angle dispersion for the k_x at 0 line, and c) is for the theta angle dispersion for k_y at 0 line, respectively. The image on b) is the 2-dimensional mapping of k_x and k_y, at E = -0.2 eV below E_F. Inset is the result of LEED image, indicating with those symmetry lines, $\overline{\Gamma X}$ and $\overline{\Gamma M}$.

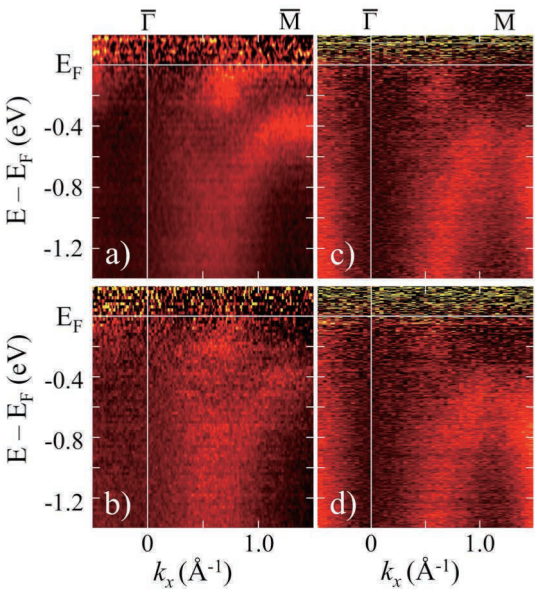

Fig. 2. Compared the experimental valence band electronic structures of $SrIrO_3$(001) and $Sr_3Ir_2O_7$(001) thin film surfaces, a) for 5 nm and b) for 2 nm of $SrIrO_3$(001), previously performed at HiSOR. The figure c) for 13.6 nm, and d) for 4.2 nm of $Sr_3Ir_2O_7$(001), all measurement at room temperature.

perpendicular to the surface but the material is weakly metallic there is some periodic dispersion along the surface normal if slight (< 0.2 eV) [3], as in Fig. 3.

References

[1] A. Dhingra, T. Komesu, S. Kumar, K. Shimada, L. Zhang, X. Hong and P. A. Dowben, *Materials Horizons* 2021, **8**, 2151–2168.

[2] S. J. Moon, H. Jin, K. W. Kim, W. S. Choi, Y. S. Lee, J. Yu, G. Cao, A. Sumi, H. Funakubo, C. Bernhard and T. W. Noh, *Phys. Rev. Lett.* 2008, **101**, 226402.

[3] Q. Wang, Y. Cao, J. A. Waugh, S. R. Park, T. F. Qi, O. B. Korneta, G. Cao and D. S. Dessau, *Phys. Rev. B* 2013, **87**, 1–6.

[4] C. Liu, S.-Y. Xu, N. Alidoust, T.-R. Chang, H. Lin, C. Dhital, S. Khadka, M. Neupane, I. Belopolski, G. Landolt, H.-T. Jeng, R. S. Markiewicz, J. H. Dil, A. Bansil, S. D. Wilson and M. Z. Hasan, *Phys. Rev. B*, 2014, **90**, 45127.

[5] P. E. Evans, T. Komesu, L. Zhang, D. F. Shao, A. J. Yost, S. Kumar, E. F. Schwier, K. Shimada, E. Y. Tsymbal, X. Hong and P. A. Dowben, *AIP Adv.*, 2020, **10**, 045027.

[6] S. Fujiyama, H. Ohsumi, T. Komesu, J. Matsuno, B.J. Kim, M. Takata, T. Arima, H. Takagi, *Phys. Rev. Lett.* 2012, **108**, 247212.

[7] B. J. Kim, H. Ohsumi, T. Komesu, S. Sakai, T. Morita, S. Fujiyama, J. Matsuno, H. Takagi, T. Arima, *Science* 2009, **323**, 1329-1332

although retaining many of the same basic features.

Fig. 3 shows the energy dependent angle-resolved photoemission of a 12.6 nm thick $Sr_3Ir_2O_7$(001) thin film. The result shows wave vector dependence both in-plane and out of plane; as a function of wave vector in-plane (i.e. k_x, as in Fig. 3 b), and also dependent on wave vector along the surface normal (i.e. k_z, as in Fig. 3 a). As seen on Fig. 3 a), the photon energy dependent results indicate that there is a small amount of periodic dispersion along the normal direction of electronic structure. This is similar to the angle-resolved photoemission results previously reported for single crystal $Sr_3Ir_2O_7$ [3]. There too, the states near Fermi level show little dispersion in wave vector

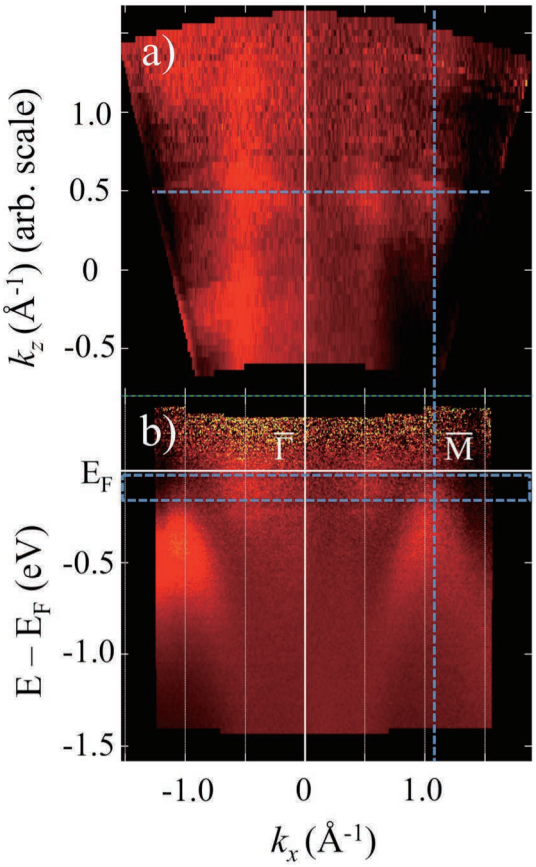

Fig. 3. The photon energy dependence of $Sr_3Ir_2O_7$(001) thin film surface, top, a) for k_z mapping of near E_F as indicated in b) with dashed area, bottom, b) for k_x direction band structure at k_z = 0.5, indicated in a), measured at room temperature.

Angle-resolved photoemission spectroscopy of Dirac nodal line superconductor $HfP_{2-x}Se_x$

Y. Nishioka[a], S. Ishizaka[b], K. Kuroda[a,c], A. Ino[d], S. Kumar[e], K. Shimada[e], H. Kito[f], I. Hase[f], S. Ishida[f], K. Oka[f], H. Fujihisa[f], Y. Gotoh[f], Y. Yoshida[f], A. Iyo[f], H. Ogino[f], H. Eisaki[f], K. Kawashima[f,g], Y. Yanagi[f,g], A. Kimura[a,c]

[a]*Graduate School of Advanced Science and Engineering, Hiroshima University, Higashi-Hiroshima 739-8526, Japan*
[b]*Graduate School of Science, Hiroshima University, Higashi-Hiroshima 739-8526, Japan*
[c]*International Institute for Sustainability with Knotted Chiral Meta Matter (WPI-SKCM²), Higashi-Hiroshima 739-8526, Japan*
[d]*Kurume Institute of Technology, Kurume 830-0052, Japan*
[e]*Hiroshima Synchrotron Radiation Center, Hiroshima University, Higashi-Hiroshima 739-0046, Japan*
[f]*National Institute of Advanced Industrial Science and Technology (AIST), Tsukuba 305-8568, Japan*
[g]*IMRA JAPAN Co., Ltd., Kariya 448-8650, Japan*

Keywords: square-net, Dirac nodal line fermions, superconductor

In recent years, nonsymmorphic *M*Si*Ch* materials (*M*=Zr, Hf, *Ch*=S, Se) have drawn significant attention as semimetals with Dirac Line Nodes (DLN) crossing the Fermi level in their band structures [1]. Recently, it has been discovered that by substituting Si with P on the glide plane, DLNs can be maintained while exhibiting superconductivity [2,3]. Investigating how such DLNs can be modulated by the elements forming the square lattice, lattice constants, and spin-orbit interactions provides detailed insights into the differences in physical properties, including superconductivity. In this study, we investigate the electronic band structures of $HfP_{2-x}Se_x$ using angle-resolved photoelectron spectroscopy (ARPES) and first principles calculations to determine the origin of the fast Dirac nodal lines. Furthermore, the effects of Dirac dispersion on the lattice constants and elemental orbitals will be addressed by comparing the P-based (superconducting $MP_{2-x}Se_x$) and Si-based (non-superconducting *M*Si*Ch*) square-net families.

Figure 1(a) shows the Fermi surface measurement result of $HfP_{1.45}Se_{0.37}$. Two large Fermi surfaces and small electron pockets at the Γ and X points are observed. The bands constituting the large Fermi surfaces exhibit gapless Dirac crossings at -0.9eV, forming a diamond-shaped ring-like DLN, as shown in Fig. 1(b)

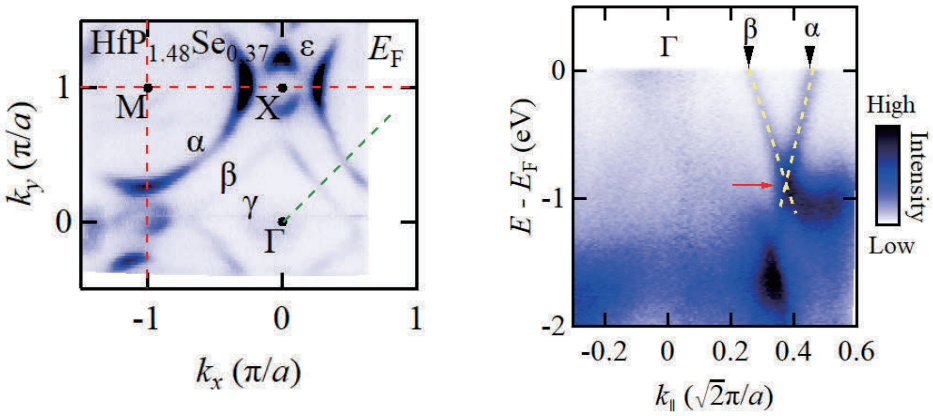

Figure 1: ARPES data of $HfP_{1.48}Se_{0.37}$, collected with $h\nu$ = 50 eV. (a) Fermi-surface map. (b) E-k plot along Γ- M line.

Since HfSiS has been reported to have a gapped DLN of around 70 meV, the DLNs in $HfP_{2-x}Se_x$ are suggested to be less affected by spin-orbit interactions. Furthermore, the Dirac velocity of $HfP_{1.45}Se_{0.37}$ reaches $v_D = 1.3\times10^6$ m/s, which is 1.1 times faster than $ZrP_{1.24}Se_{0.57}$ and 1.7 times faster than HfSiS. This indicates that factors other than Si contribute to the acceleration of the Dirac electrons due to the larger lattice constant of the P square lattice compared to Si. This study demonstrates that $MP_{2-x}Se_x$ with the P square lattice is a superconductor with fast line-node-type Dirac electrons and is less affected by spin-orbit interactions, opening up possibilities for novel material studies.

The experiment was carried out at BL1 of HiSOR (Proposal Nos. 22AG039, 22AG040). This work was financially supported by JSPS KAKENHI (Grants No. 17H06138, No. 18H03683).

REFERENCES

1. L. M. Schoop *et al*., Nat. Commun. **7**, 11696 (2016).
2. H. Kito *et al*., J. Phys. Soc. Jpn. **83**, 074713 (2014).
3. S. Ishizaka *et al*., Phys. Rev. B **105**, L121103(2022).

Realization of Practical Eightfold Fermions and Fourfold van Hove Singularity in $TaCo_2Te_2$

Hongtao Rong[1*], Zhenqiao Huang[1,7*], Xin Zhang[2,8*], Shiv Kumar[3*], Fayuang Zhang[1], Chengcheng Zhang[1], Yuan Wang[1], Zhanyang Hao[1], Yongqing Cai[1], Le Wang[1], Cai Liu[1], Xiao-Ming Ma[1], Shu Guo[1], Bing Shen[4], Yi Liu[5], Shengtao Cui[5], Kenya Shimada[3], Quansheng Wu[6,10], Junhao Lin[1], Yugui Yao[2,8], Zhiwei Wang[2,8,9#], Hu Xu[1#], and Chaoyu Chen[1#]

[1] *Shenzhen Institute for Quantum Science and Engineering (SIQSE) and Department of Physics, Southern University of Science and Technology (SUSTech), Shenzhen 518055, China.*

[2] *Centre for Quantum Physics, Key Laboratory of Advanced Optoelectronic Quantum Architecture and Measurement, School of Physics, Beijing Institute of Technology, Beijing 100081, China.*

[3] *Hiroshima Synchrotron Radiation Centre, Hiroshima University, Higashi-Hiroshima, Hiroshima 739-0046, Japan.*

[4] *School of Physics, Sun Yat-Sen University, Guangzhou 510275, China.*

[5] *National Synchrotron Radiation Laboratory, University of Science and Technology of China, Hefei, Anhui 230029, China.*

[6] *Beijing National Laboratory for Condensed Matter Physics, and Institute of Physics, Chinese Academy of Sciences, Beijing 100190, China.*

[7] *Department of Physics, The Hong Kong University of Science and Technology, Clear Water Bay, Hong Kong, China.*

[8] *Beijing Key Lab of Nanophotonics and Ultrafifine Optoelectronic Systems, Beijing Institute of Technology, Beijing 100081, China.*

[9] *Material Science Center, Yangtze Delta Region Academy of Beijing Institute of Technology, Jiaxing 314011, China.*

[10] *University of Chinese Academy of Sciences, Beijing 100049, China.*

Keywords: Topological states, eightfold fermions, fourfold van Hove singularity, hourglass fermion

Searching for new elementary excitation/quasiparticles is a key pursuit of condensed matter physics. In the past decades, Weyl and Dirac type low-energy quasiparticles, in analog to relativistic massless Weyl and Dirac fermions in high-energy physics, have been realized based on materials such as graphene, topological insulator, and Weyl/Dirac semimetal. Moreover, the 230 space groups in condensed matter physics impose fewer constraints on the allowed types of fermions. New fermionic quasiparticles beyond high-energy physics, including threefold, sixfold, and eightfold fermions, can emerge. So far, while Weyl (twofold), threefold, Dirac (fourfold), and sixfold quasiparticles have been observed in quantum materials[1-12], eightfold fermions remain to be realized. Based on a nonsymmorphic crystal $TaCo_2Te_2$, we provide a clear spectroscopic signature of eightfold degenerate fermions protected by the combination of crystalline and time-reversal symmetry.

We establish $TaCo_2Te_2$ as a conjoint topological and quantum critical platform with handful stimuli available to tune its physical properties. Chemical substitution or applying strain may introduce long range magnetic order and magnetic quantum critical point is expected. The negligible SOC leads to the practical realization of eightfold fermions, which, according to theoretical analysis, serves as a topological quantum critical point. Symmetry breaking via magnetic field or uniaxial strain may lead to various topologically trivial or nontrivial phases such as Dirac point, Weyl point or nodal lines. Consequently, our findings will stimulate broad research interest from subfields of condensed matter physics such as quantum transport, strong correlation, material synthesis and topological states of matter.

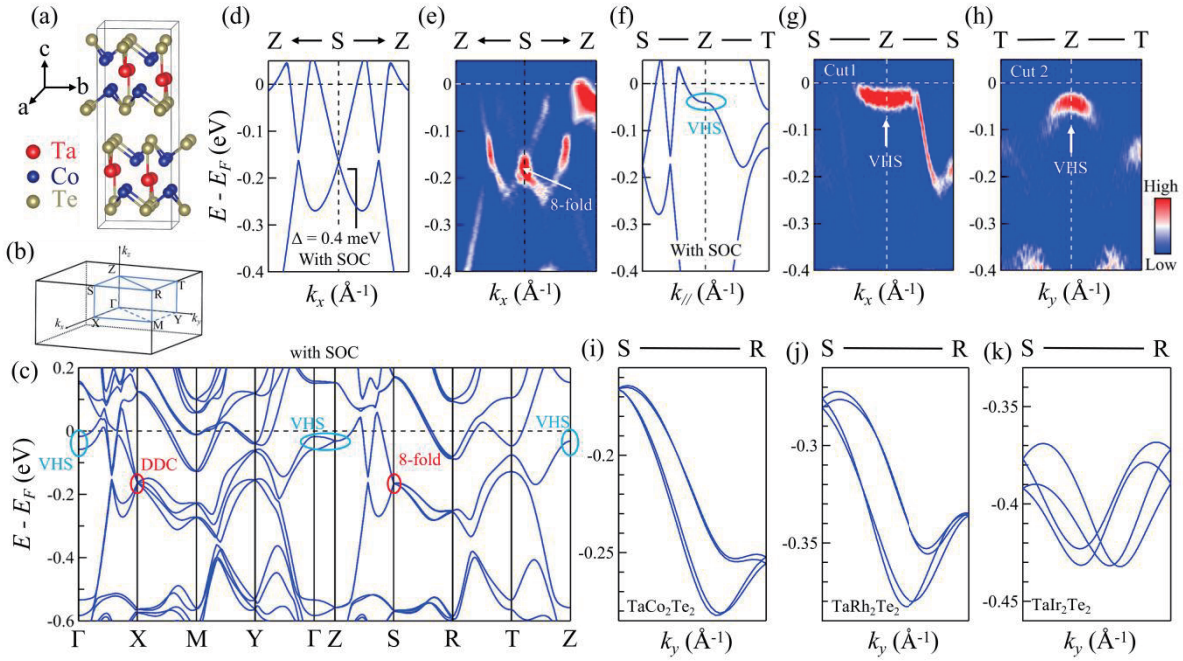

FIGURE 1. Crystal structure, eightfold fermion, fourfold van Hove singularity and hourglass in $TaCo_2Te_2$. (a) Crystal structure. (b) 3D bulk BZ. (c) DFT calculated dispersions along the high-symmetry path with considering SOC. (d, e) DFT calculated dispersions and ARPES dispersion around eightfold fermion. (f-h) DFT calculated dispersions and ARPES dispersion around van Hove singularity. (i-k) DFT predicted hourglass fermions in TaT_2Te_2 (T= Co, Rh and Ir).

REFERENCES

1. A. Alexandradinata, Zhijun Wang & B. Andrei Bernevig. *Physical Review X* **6**, 021008 (2016)
2. B. Bradlyn, J. Cano, Z. Wang, M. G. Vergniory, C. Felser, R. J. Cava & B. A. Bernevig. *Science* **353**, 5037 (2016)
3. S. M. Huang, S. Y. Xu, I. Belopolski, C. C. Lee, G. Chang, T. R. Chang, B. Wang, N. Alidoust, G. Bian, M. Neupane, D. Sanchez, H. Zheng, H. T. Jeng, A. Bansil, T. Neupert, H. Lin & M. Z. Hasan. *Proc Natl Acad Sci USA* **113**, 1180-1185 (2016)
4. Z. Wang, A. Alexandradinata, R. J. Cava & B. A. Bernevig. *Nature* **532**, 189-194 (2016)
5. Hongming Weng, Chen Fang, Zhong Fang & Xi Dai. *Physical Review B* **93**, 241202 (2016)
6. B. J. Wieder, Y. Kim, A. M. Rappe & C. L. Kane. *Phys Rev Lett* **116**, 186402 (2016)
7. Ziming Zhu, Georg W. Winkler, QuanSheng Wu, Ju Li & Alexey A. Soluyanov. *Physical Review X* **6**, 031003 (2016)
8. Qihang Liu & Alex Zunger. *Physical Review X* **7**, 021019 (2017)
9. Benjamin J. Wieder, Barry Bradlyn, Zhijun Wang, Jennifer Cano, Youngkuk Kim, Hyeong-Seok D. Kim, Andrew M. Rappe, C. L. Kane & B. Andrei Bernevig. *Science* **361**, 246-251 (2018)
10. Weikang Wu, Zhi-Ming Yu, Xiaoting Zhou, Y. X. Zhao & Shengyuan A. Yang. *Physical Review B* **101**, 205134 (2020)
11. P. J. Guo, Y. W. Wei, K. Liu, Z. X. Liu & Z. Y. Lu. *Phys Rev Lett* **127**, 176401 (2021)
12. Jennifer Cano, Barry Bradlyn & M. G. Vergniory. *APL Materials* **7**, 101125 (2019)

Band structure study of $MnBi_2Te_4$ growth via the chemical vapor transport method

Yuan Wang[1], Hongtao Rong[1], Fayuan Zhang[1], Zhanyang Hao[1], Yongqing Cai[1], Ni Ni[2], and Chaoyu Chen[1]

[1] *Shenzhen Institute for Quantum Science and Engineering (SIQSE) and Department of Physics, Southern University of Science and Technology (SUSTech), Shenzhen 518055, China.*

[2] *Department of Physics and Astronomy and California NanoSystems Institute, University of California, Los Angeles, California 90095, USA*

Keywords: Intrinsic magnetic topological insulator, topological surface state, band structure

As the first intrinsic magnetic topological insulator, the band structure of $MnBi_2Te_4$ has been deeply studied [1-6]. The topological surface state inside the bulk gap is the focus of attention. In the early stage, a considerable gap was found for the topological surface state Dirac cone with temperature-independent behavior [1,7,8]. However, the subsequent ARPES(Angle-resolved photoemission spectroscopy) work revealed the nearly gapless behavior of topological surface states [2-6,9-13] through the system's photon energy-dependent measurement and higher energy and momentum resolution, showing sample and position dependence. The experimentally observed Dirac gap size from vanishing to tens of millivolts is much smaller than the theoretical expectation [1,14-16]. These behaviors indicate that the effective magnetic moment felt by the topological surface state is greatly reduced, which may be caused by surface magnetic reconstruction or topological surface state redistribution. At present, several mechanisms that may lead to one of these two phenomena have been proposed, but none of them have been experimentally verified.

$MnBi_2Te_4$ provides a platform for studying the interaction between band topology and magnetism and the resulting novel phenomena. We performed measurements using μ-Laser ARPES@HiSOR with ultra-high energy resolution. Four different polarization states of light source were employed to measure the band structures. We observed that the Dirac point is closer to the Fermi surface compared to the sample grown with flux, which is consistent with the findings of our collaborator[17]. Additionally, the high-quality band structures allowed us to distinguish between bulk state and surface state. The clear surface state exhibited a gap of approximately 47 meV. Combining these results with the transport data previously published by our collaborator, we will conduct further analysis and research.

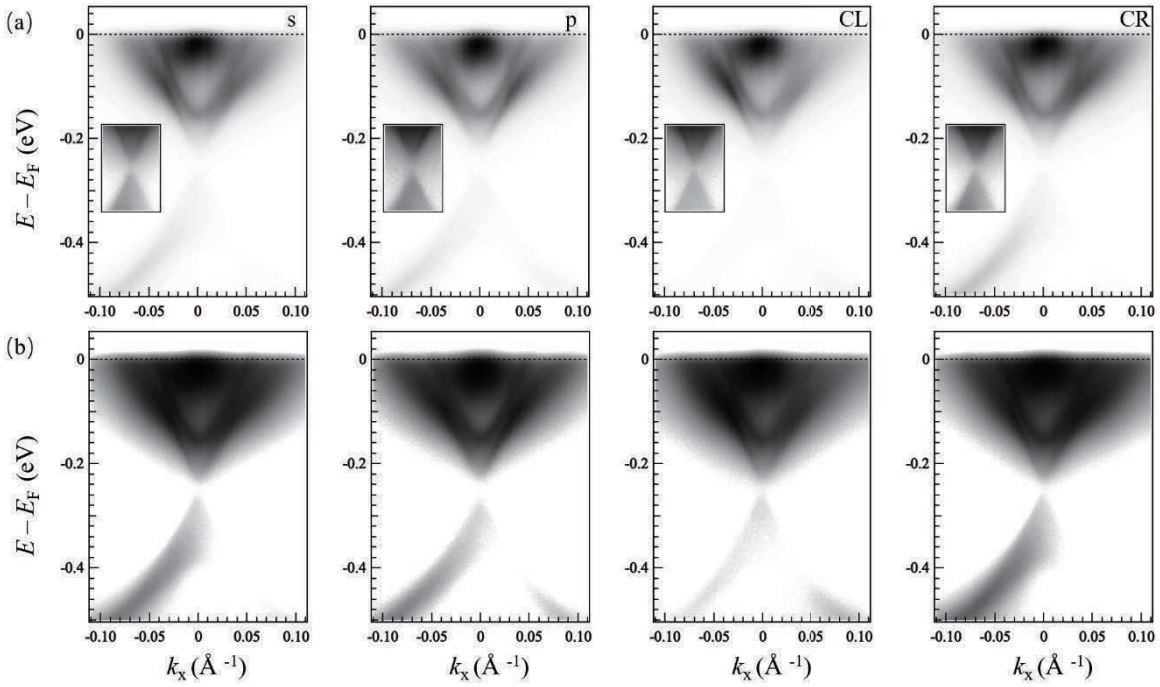

FIGURE 1. ARPES spectra measured at four different polarization states of light source.

REFERENCES

[1] M. M. Otrokov, Klimovskikh, II, H. Bentmann, D. Estyunin, A. Zeugner, Z. S. Aliev, S. Gass, A. U. B. Wolter, A. V. Koroleva, A. M. Shikin, M. Blanco-Rey, M. Hoffmann, I. P. Rusinov, A. Y. Vyazovskaya, S. V. Eremeev, Y. M. Koroteev, V. M. Kuznetsov, F. Freyse, J. Sanchez-Barriga, I. R. Amiraslanov, M. B. Babanly, N. T. Mamedov, N. A. Abdullayev, V. N. Zverev, A. Alfonsov, V. Kataev, B. Buchner, E. F. Schwier, S. Kumar, A. Kimura, L. Petaccia, G. Di Santo, R. C. Vidal, S. Schatz, K. Kissner, M. Unzelmann, C. H. Min, S. Moser, T. R. F. Peixoto, F. Reinert, A. Ernst, P. M. Echenique, A. Isaeva & E. V. Chulkov. Prediction and observation of an antiferromagnetic topological insulator. *Nature* **576**, 416-422, doi:10.1038/s41586-019-1840-9 (2019).

[2] Yu-Jie Hao, Pengfei Liu, Yue Feng, Xiao-Ming Ma, Eike F. Schwier, Masashi Arita, Shiv Kumar, Chaowei Hu, Rui'e Lu, Meng Zeng, Yuan Wang, Zhanyang Hao, Hong-Yi Sun, Ke Zhang, Jiawei Mei, Ni Ni, Liusuo Wu, Kenya Shimada, Chaoyu Chen, Qihang Liu & Chang Liu. Gapless Surface Dirac Cone in Antiferromagnetic Topological Insulator MnBi2Te4. *Physical Review X* **9**, 041038, doi:10.1103/PhysRevX.9.041038 (2019).

[3] Y. J Chen, L. X Xu, J. H Li, Y. W Li, H. Y Wang, C. F Zhang, H. Li, Y. Wu, A. J Liang, C. Chen, S. W Jung, C. Cacho, Y. H Mao, S. Liu, M. X Wang, Y. F Guo, Y. Xu, Z. K Liu, L. X Yang & Y. L Chen. Topological Electronic Structure and Its Temperature Evolution in Antiferromagnetic Topological Insulator MnBi2Te4. *Physical Review X* **9**, 041040, doi:10.1103/PhysRevX.9.041040 (2019).

[4] Hang Li, Shun-Ye Gao, Shao-Feng Duan, Yuan-Feng Xu, Ke-Jia Zhu, Shang-Jie Tian, Jia-Cheng Gao, Wen-Hui Fan, Zhi-Cheng Rao, Jie-Rui Huang, Jia-Jun Li, Da-Yu Yan, Zheng-Tai Liu, Wan-Ling Liu, Yao-Bo Huang, Yu-Liang Li, Yi Liu, Guo-Bin Zhang, Peng Zhang, Takeshi Kondo, Shik Shin, He-Chang Lei, You-Guo Shi, Wen-Tao Zhang, Hong-Ming Weng, Tian Qian & Hong Ding. Dirac Surface States in Intrinsic Magnetic Topological Insulators EuSn2As2 and MnBi2nTe3n+1. *Physical Review X* **9**, 041039, doi:10.1103/PhysRevX.9.041039 (2019).

[5] A. Liang, C. Chen, H. Zheng, W. Xia, K. Huang, L. Wei, H. Yang, Y. Chen, X. Zhang, X. Xu, M. Wang, Y. Guo, L. Yang, Z. Liu & Y. Chen. Approaching a Minimal Topological Electronic Structure in Antiferromagnetic Topological Insulator MnBi2Te4 via Surface Modification. *Nano Lett* **22**, 4307-4314, doi:10.1021/acs.nanolett.1c04930 (2022).

[6] Runzhe Xu, Yunhe Bai, Jingsong Zhou, Jiaheng Li, Xu Gu, Na Qin, Zhongxu Yin, Xian Du, Qinqin Zhang, Wenxuan Zhao, Yidian Li, Yang Wu, Cui Ding, Lili Wang, Aiji Liang, Zhongkai Liu, Yong Xu, Xiao Feng, Ke He, Yulin Chen & Lexian Yang. Evolution of the Electronic Structure of Ultrathin MnBi2Te4 Films. *Nano Letters* **22**, 6320-6327, doi:10.1021/acs.nanolett.2c02034 (2022).

[7] R. C. Vidal, H. Bentmann, T. R. F. Peixoto, A. Zeugner, S. Moser, C. H. Min, S. Schatz, K. Kißner, M. Ünzelmann, C. I. Fornari, H. B. Vasili, M. Valvidares, K. Sakamoto, D. Mondal, J. Fujii, I. Vobornik, S. Jung, C. Cacho, T. K. Kim, R. J. Koch, C. Jozwiak, A. Bostwick, J. D. Denlinger, E. Rotenberg, J. Buck, M. Hoesch, F. Diekmann, S. Rohlf, M. Kalläne, K. Rossnagel, M. M. Otrokov, E. V. Chulkov, M. Ruck, A. Isaeva & F. Reinert. Surface states and Rashba-type spin polarization in antiferromagnetic MnBi2Te4 (0001). *Physical Review B* **100**, doi:10.1103/PhysRevB.100.121104 (2019).

[8] Seng Huat Lee, Yanglin Zhu, Yu Wang, Leixin Miao, Timothy Pillsbury, Hemian Yi, Susan Kempinger, Jin Hu, Colin A.

Heikes, P. Quarterman, William Ratcliff, Julie A. Borchers, Heda Zhang, Xianglin Ke, David Graf, Nasim Alem, Cui-Zu Chang, Nitin Samarth & Zhiqiang Mao. Spin scattering and noncollinear spin structure-induced intrinsic anomalous Hall effect in antiferromagnetic topological insulator MnBi2Te4. *Physical Review Research* **1**, doi:10.1103/PhysRevResearch.1.012011 (2019).

[9] Yong Hu, Lixuan Xu, Mengzhu Shi, Aiyun Luo, Shuting Peng, Z. Y. Wang, J. J. Ying, T. Wu, Z. K. Liu, C. F. Zhang, Y. L. Chen, G. Xu, X. H. Chen & J. F. He. Universal gapless Dirac cone and tunable topological states in (MnBi2Te4)m(Bi2Te3)n heterostructures. *Physical Review B* **101**, 161113(R) (2020).

[10] D. Nevola, H. X. Li, J. Q. Yan, R. G. Moore, H. N. Lee, H. Miao & P. D. Johnson. Coexistence of Surface Ferromagnetism and a Gapless Topological State in MnBi2Te4. *Phys Rev Lett* **125**, 117205, doi:10.1103/PhysRevLett.125.117205 (2020).

[11] A. M. Shikin, D. A. Estyunin, Klimovskikh, II, S. O. Filnov, E. F. Schwier, S. Kumar, K. Miyamoto, T. Okuda, A. Kimura, K. Kuroda, K. Yaji, S. Shin, Y. Takeda, Y. Saitoh, Z. S. Aliev, N. T. Mamedov, I. R. Amiraslanov, M. B. Babanly, M. M. Otrokov, S. V. Eremeev & E. V. Chulkov. Nature of the Dirac gap modulation and surface magnetic interaction in axion antiferromagnetic topological insulator MnBi2Te4. *Sci Rep* **10**, 13226, doi:10.1038/s41598-020-70089-9 (2020).

[12] Przemyslaw Swatek, Yun Wu, Lin-Lin Wang, Kyungchan Lee, Benjamin Schrunk, Jiaqiang Yan & Adam Kaminski. Gapless Dirac surface states in the antiferromagnetic topological insulator MnBi2Te4. *Physical Review B* **101**, 161109, doi:10.1103/PhysRevB.101.161109 (2020).

[13] A. M. Shikin, D. A. Estyunin, N. L. Zaitsev, D. Glazkova, I. I. Klimovskikh, S. O. Filnov, A. G. Rybkin, E. F. Schwier, S. Kumar, A. Kimura, N. Mamedov, Z. Aliev, M. B. Babanly, K. Kokh, O. E. Tereshchenko, M. M. Otrokov, E. V. Chulkov, K. A. Zvezdin & A. K. Zvezdin. Sample-dependent Dirac-point gap in MnBi2Te4 and its response to applied surface charge: A combined photoemission and ab initio study. *Physical Review B* **104**, 115168, doi:10.1103/PhysRevB.104.115168 (2021).

[14] D. Zhang, M. Shi, T. Zhu, D. Xing, H. Zhang & J. Wang. Topological Axion States in the Magnetic Insulator MnBi2Te4 with the Quantized Magnetoelectric Effect. *Phys Rev Lett* **122**, 206401, doi:10.1103/PhysRevLett.122.206401 (2019).

[15] M. M. Otrokov, I. P. Rusinov, M. Blanco-Rey, M. Hoffmann, A. Y. Vyazovskaya, S. V. Eremeev, A. Ernst, P. M. Echenique, A. Arnau & E. V. Chulkov. Unique Thickness-Dependent Properties of the van der Waals Interlayer Antiferromagnet MnBi2Te4 Films. *Phys Rev Lett* **122**, 107202, doi:10.1103/PhysRevLett.122.107202 (2019).

[16] Jiaheng Li, Yang Li, Shiqiao Du, Zun Wang, Bing-Lin Gu, Shou-Cheng Zhang, Ke He, Wenhui Duan & Yong Xu. Intrinsic magnetic topological insulators in van der Waals layered MnBi2Te4-family materials. *Science Advances* **5**, eaaw5685, doi:10.1126/sciadv.aaw5685 (2019).

[17] Chaowei Hu, Anyuan Gao , Bryan Stephen Berggren , Hong Li, Rafa Kurleto, Dushyant Narayan, Ilija Zeljkovic, Dan Dessau, Suyang Xu, and Ni Ni. Growth, characterization, and Chern insulator state in MnBi2Te4 via the chemical vapor transport method. PHYSICAL REVIEW MATERIALS 5, 124206 (2021)

Photoemission study on the electronic structure of an antiferromagnetic semimetal

Yongqing Cai[1], Zhanyang Hao[1], Hongtao Rong[1], Fayuan Zhang[1], Yuan Wang[1] and Chaoyu Chen[1]

[1] *Shenzhen Institute for Quantum Science and Engineering (SIQSE) and Department of Physics, Southern University of Science and Technology (SUSTech), Shenzhen 518055, China.*

Keywords: antiferromagnetic semimetal, angle-resolved photoemission spectroscopy, flat band

Antiferromagnetic materials possess significant scientific interest due to their diverse spin arrangements, opening up a wide range of potential applications in areas such as data storage, electronic devices, quantum computing, and communication technologies [1]. The exploration of antiferromagnetic materials in the realm of quantum computing holds promise for advancing the field and enabling new computational capabilities. Moreover, recent discoveries have revealed that many antiferromagnetic compounds exhibit nontrivial topological electronic and spin states[2-4]. In order to advance these materials and discover new ones, it is crucial to comprehend the magnetic interactions at play. Eu-based antiferromagnetic materials have garnered significant interest in recent years due to the intriguing interplay between magnetism and topological states[5-9]. These materials exhibit a complex relationship between their antiferromagnetic order and the emergence of nontrivial topological electronic and spin states.

In this work, by conducting high-resolution angle-resolved photoemission spectroscopy (ARPES) measurements of BL-1 in HiSOR, we systematically investigate the electronic structure of a Eu-based antiferromagnetic semimetal, $EuGa_4$. As shown in Fig. 1(a), $EuGa_4$ crystallizes in a centrosymmetric tetragonal $BaAl_4$-type structure (space group I4/mmm), exhibiting antiferromagnetic order below the Néel temperature (T_N) of 15 K. Judging from the Fermi surface geometry, we align the ARPES momentum cut to $\overline{\Gamma}-\overline{X}$ high-symmetry path ($k_y = 0$ path in Fig. 1(c)) and perform photon energy-dependent measurement for a photon energy range of $60-160\ eV$. The clear periodic dispersion enables us to identify the bulk Γ and A points, as shown in Fig. 1(b). The Fermi surfaces and band structures along high-symmetry direction at $k_z = 0$ and π are demonstrated in Figs. 1(c-f). Around the Brillouin zone center, the Fermi surface sheet is composed of an inner circular hole pocket and an outer diamond-like electron pocket. Remarkably, a pronounced flat band is observed at around 1.5 eV below E_F across the whole momentum area. To confirm the intrinsic nature of the flat band and exclude the nondispersive core level spectra excited by twice the photon energy, it is necessary to examine whether the binding energy position of the flat band changes with the photon energy. As shown in Figs. 1(g-h), the ARPES spectra with both photon energies of $120\ eV$ and $121\ eV$ demonstrate a nearly non-dispersive band at $\sim 1.5\ eV$ below E_F. The excitation energy independence of this band eliminates the possibility of core level spectra excited by twice the photon energy and reveals its intrinsic nature. The flat band is located far below the Fermi level, rendering its physical

responses hardly observable. Manipulating the flat band to Fermi level calls for further investigation.

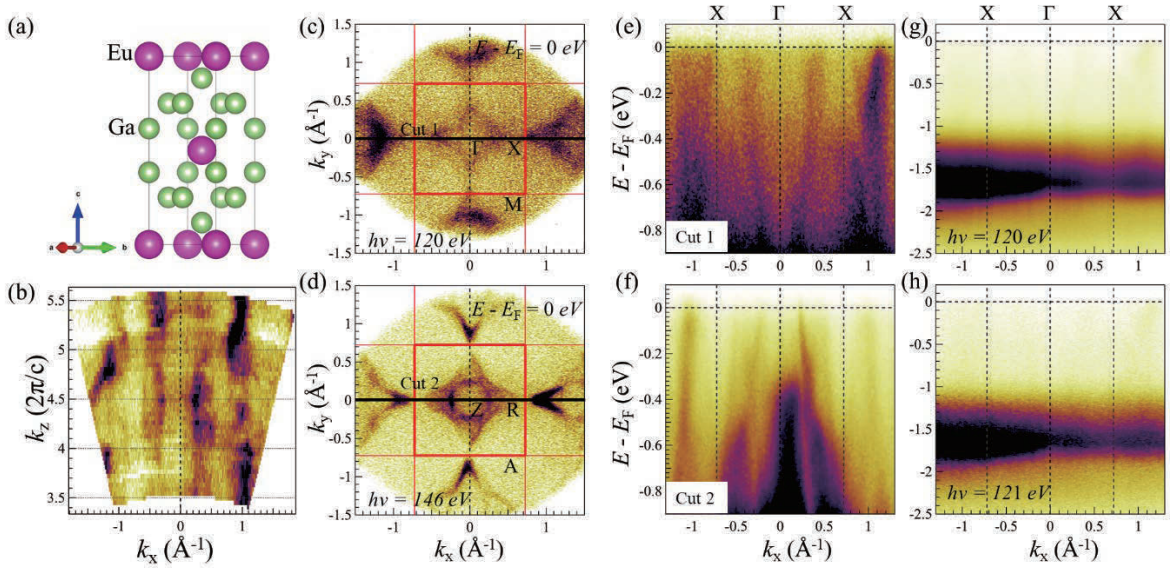

Fig. 1 General electronic structure of $EuGa_4$ measured by ARPES.

Reference:

1. Žutić I, Fabian J, Das Sarma S. Spintronics: Fundamentals and applications. *Rev. Mod. Phys.* 2004, **76**(2)**:** 323-410.
2. Otrokov MM*, et al.* Prediction and observation of an antiferromagnetic topological insulator. *Nature* 2019, **576**(7787)**:** 416-422.
3. Kurumaji T*, et al.* Skyrmion lattice with a giant topological Hall effect in a frustrated triangular-lattice magnet. *Science* 2019, **365**(6456)**:** 914-918.
4. Hirschberger M*, et al.* The chiral anomaly and thermopower of Weyl fermions in the half-Heusler GdPtBi. *Nat Mater* 2016, **15**(11)**:** 1161-1165.
5. Riberolles SXM*, et al.* Magnetic crystalline-symmetry-protected axion electrodynamics and field-tunable unpinned Dirac cones in EuIn(2)As(2). *Nat Commun* 2021, **12**(1)**:** 999.
6. Rahn MC*, et al.* Coupling of magnetic order and charge transport in the candidate Dirac semimetal EuCd2As2. *Phys Rev B* 2018, **97**(21).
7. Li H*, et al.* Dirac Surface States in Intrinsic Magnetic Topological Insulators EuSn2As2 and MnBi2nTe3n+1. *Phys. Rev. X* 2019, **9**(4).
8. Jo NH*, et al.* Manipulating magnetism in the topological semimetal EuCd2As2. *Phys Rev B* 2020, **101**(14).
9. Hao Y-J*, et al.* Gapless Surface Dirac Cone in Antiferromagnetic Topological Insulator MnBi2Te4. *Phys. Rev. X* 2019, **9**(4).

Band structure study of $MnBi_2Te_4$ growth via the chemical vapor transport method

Yuan Wang[1], Hongtao Rong[1], Fayuan Zhang[1], Zhanyang Hao[1], Yongqing Cai[1], Ni Ni[2], and Chaoyu Chen[1]

[1] *Shenzhen Institute for Quantum Science and Engineering (SIQSE) and Department of Physics, Southern University of Science and Technology (SUSTech), Shenzhen 518055, China.*

[2] *Department of Physics and Astronomy and California NanoSystems Institute, University of California, Los Angeles, California 90095, USA*

Keywords: Intrinsic magnetic topological insulator, topological surface state, band structure

As the first intrinsic magnetic topological insulator, the band structure of $MnBi_2Te_4$ has been deeply studied [1-6]. The topological surface state inside the bulk gap is the focus of attention. In the early stage, a considerable gap was found for the topological surface state Dirac cone with temperature-independent behavior [1,7,8]. However, the subsequent ARPES(Angle-resolved photoemission spectroscopy) work revealed the nearly gapless behavior of topological surface states [2-6,9-13] through the system's photon energy-dependent measurement and higher energy and momentum resolution, showing sample and position dependence. The experimentally observed Dirac gap size from vanishing to tens of millivolts is much smaller than the theoretical expectation [1,14-16]. These behaviors indicate that the effective magnetic moment felt by the topological surface state is greatly reduced, which may be caused by surface magnetic reconstruction or topological surface state redistribution. At present, several mechanisms that may lead to one of these two phenomena have been proposed, but none of them have been experimentally verified.

$MnBi_2Te_4$ provides a platform for studying the interaction between band topology and magnetism and the resulting novel phenomena. We performed measurements using μ-Laser ARPES@HiSOR with ultra-high energy resolution. Four different polarization states of light source were employed to measure the band structures. We observed that the Dirac point is closer to the Fermi surface compared to the sample grown with flux, which is consistent with the findings of our collaborator[17]. Additionally, the high-quality band structures allowed us to distinguish between bulk state and surface state. The clear surface state exhibited a gap of approximately 47 meV. Combining these results with the transport data previously published by our collaborator, we will conduct further analysis and research.

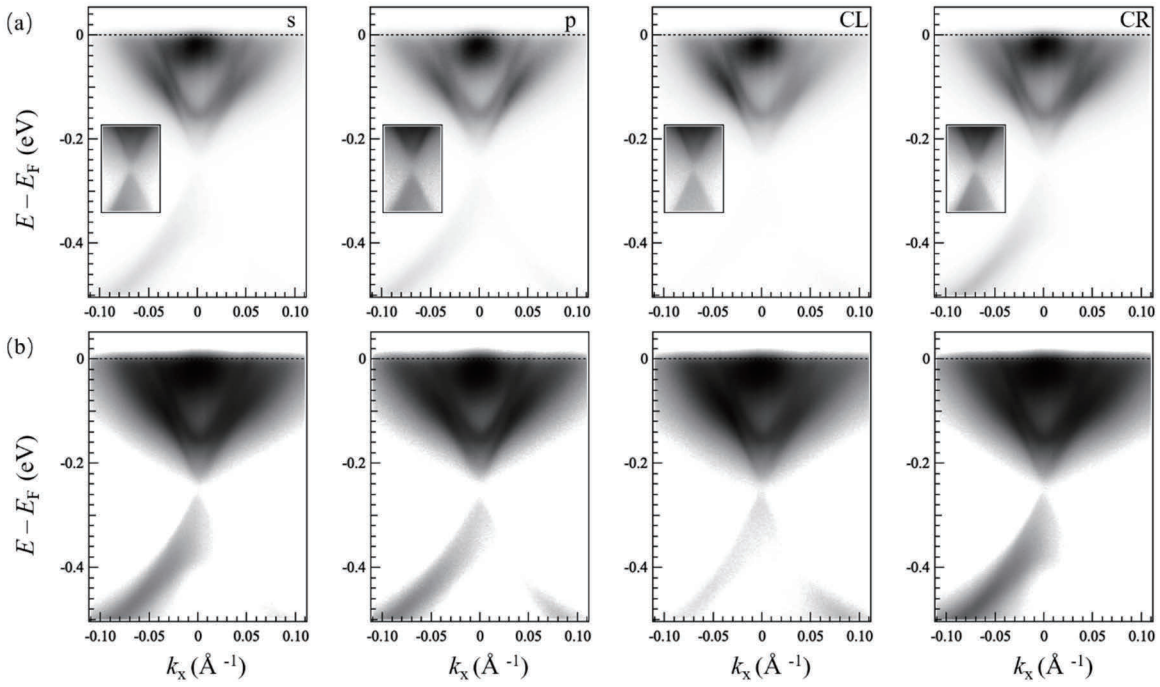

FIGURE 1. ARPES spectra measured at four different polarization states of light source.

REFERENCES

[1] M. M. Otrokov, Klimovskikh, II, H. Bentmann, D. Estyunin, A. Zeugner, Z. S. Aliev, S. Gass, A. U. B. Wolter, A. V. Koroleva, A. M. Shikin, M. Blanco-Rey, M. Hoffmann, I. P. Rusinov, A. Y. Vyazovskaya, S. V. Eremeev, Y. M. Koroteev, V. M. Kuznetsov, F. Freyse, J. Sanchez-Barriga, I. R. Amiraslanov, M. B. Babanly, N. T. Mamedov, N. A. Abdullayev, V. N. Zverev, A. Alfonsov, V. Kataev, B. Buchner, E. F. Schwier, S. Kumar, A. Kimura, L. Petaccia, G. Di Santo, R. C. Vidal, S. Schatz, K. Kissner, M. Unzelmann, C. H. Min, S. Moser, T. R. F. Peixoto, F. Reinert, A. Ernst, P. M. Echenique, A. Isaeva & E. V. Chulkov. Prediction and observation of an antiferromagnetic topological insulator. *Nature* **576**, 416-422, doi:10.1038/s41586-019-1840-9 (2019).

[2] Yu-Jie Hao, Pengfei Liu, Yue Feng, Xiao-Ming Ma, Eike F. Schwier, Masashi Arita, Shiv Kumar, Chaowei Hu, Rui'e Lu, Meng Zeng, Yuan Wang, Zhanyang Hao, Hong-Yi Sun, Ke Zhang, Jiawei Mei, Ni Ni, Liusuo Wu, Kenya Shimada, Chaoyu Chen, Qihang Liu & Chang Liu. Gapless Surface Dirac Cone in Antiferromagnetic Topological Insulator MnBi2Te4. *Physical Review X* **9**, 041038, doi:10.1103/PhysRevX.9.041038 (2019).

[3] Y. J Chen, L. X Xu, J. H Li, Y. W Li, H. Y Wang, C. F Zhang, H. Li, Y. Wu, A. J Liang, C. Chen, S. W Jung, C. Cacho, Y. H Mao, S. Liu, M. X Wang, Y. F Guo, Y. Xu, Z. K Liu, L. X Yang & Y. L Chen. Topological Electronic Structure and Its Temperature Evolution in Antiferromagnetic Topological Insulator MnBi2Te4. *Physical Review X* **9**, 041040, doi:10.1103/PhysRevX.9.041040 (2019).

[4] Hang Li, Shun-Ye Gao, Shao-Feng Duan, Yuan-Feng Xu, Ke-Jia Zhu, Shang-Jie Tian, Jia-Cheng Gao, Wen-Hui Fan, Zhi-Cheng Rao, Jie-Rui Huang, Jia-Jun Li, Da-Yu Yan, Zheng-Tai Liu, Wan-Ling Liu, Yao-Bo Huang, Yu-Liang Li, Yi Liu, Guo-Bin Zhang, Peng Zhang, Takeshi Kondo, Shik Shin, He-Chang Lei, You-Guo Shi, Wen-Tao Zhang, Hong-Ming Weng, Tian Qian & Hong Ding. Dirac Surface States in Intrinsic Magnetic Topological Insulators EuSn2As2 and MnBi2nTe3n+1. *Physical Review X* **9**, 041039, doi:10.1103/PhysRevX.9.041039 (2019).

[5] A. Liang, C. Chen, H. Zheng, W. Xia, K. Huang, L. Wei, H. Yang, Y. Chen, X. Zhang, X. Xu, M. Wang, Y. Guo, L. Yang, Z. Liu & Y. Chen. Approaching a Minimal Topological Electronic Structure in Antiferromagnetic Topological Insulator MnBi2Te4 via Surface Modification. *Nano Lett* **22**, 4307-4314, doi:10.1021/acs.nanolett.1c04930 (2022).

[6] Runzhe Xu, Yunhe Bai, Jingsong Zhou, Jiaheng Li, Xu Gu, Na Qin, Zhongxu Yin, Xian Du, Qinqin Zhang, Wenxuan Zhao, Yidian Li, Yang Wu, Cui Ding, Lili Wang, Aiji Liang, Zhongkai Liu, Yong Xu, Xiao Feng, Ke He, Yulin Chen & Lexian Yang. Evolution of the Electronic Structure of Ultrathin MnBi2Te4 Films. *Nano Letters* **22**, 6320-6327, doi:10.1021/acs.nanolett.2c02034 (2022).

[7] R. C. Vidal, H. Bentmann, T. R. F. Peixoto, A. Zeugner, S. Moser, C. H. Min, S. Schatz, K. Kißner, M. Ünzelmann, C. I. Fornari, H. B. Vasili, M. Valvidares, K. Sakamoto, D. Mondal, J. Fujii, I. Vobornik, S. Jung, C. Cacho, T. K. Kim, R. J. Koch, C. Jozwiak, A. Bostwick, J. D. Denlinger, E. Rotenberg, J. Buck, M. Hoesch, F. Diekmann, S. Rohlf, M. Kalläne, K. Rossnagel, M. M. Otrokov, E. V. Chulkov, M. Ruck, A. Isaeva & F. Reinert. Surface states and Rashba-type spin polarization in antiferromagnetic MnBi2Te4 (0001). *Physical Review B* **100**, doi:10.1103/PhysRevB.100.121104 (2019).

[8] Seng Huat Lee, Yanglin Zhu, Yu Wang, Leixin Miao, Timothy Pillsbury, Hemian Yi, Susan Kempinger, Jin Hu, Colin A.

Heikes, P. Quarterman, William Ratcliff, Julie A. Borchers, Heda Zhang, Xianglin Ke, David Graf, Nasim Alem, Cui-Zu Chang, Nitin Samarth & Zhiqiang Mao. Spin scattering and noncollinear spin structure-induced intrinsic anomalous Hall effect in antiferromagnetic topological insulator MnBi2Te4. *Physical Review Research* **1**, doi:10.1103/PhysRevResearch.1.012011 (2019).

[9] Yong Hu, Lixuan Xu, Mengzhu Shi, Aiyun Luo, Shuting Peng, Z. Y. Wang, J. J. Ying, T. Wu, Z. K. Liu, C. F. Zhang, Y. L. Chen, G. Xu, X. H. Chen & J. F. He. Universal gapless Dirac cone and tunable topological states in (MnBi2Te4)m(Bi2Te3)n heterostructures. *Physical Review B* **101**, 161113(R) (2020).

[10] D. Nevola, H. X. Li, J. Q. Yan, R. G. Moore, H. N. Lee, H. Miao & P. D. Johnson. Coexistence of Surface Ferromagnetism and a Gapless Topological State in MnBi2Te4. *Phys Rev Lett* **125**, 117205, doi:10.1103/PhysRevLett.125.117205 (2020).

[11] A. M. Shikin, D. A. Estyunin, Klimovskikh, II, S. O. Filnov, E. F. Schwier, S. Kumar, K. Miyamoto, T. Okuda, A. Kimura, K. Kuroda, K. Yaji, S. Shin, Y. Takeda, Y. Saitoh, Z. S. Aliev, N. T. Mamedov, I. R. Amiraslanov, M. B. Babanly, M. M. Otrokov, S. V. Eremeev & E. V. Chulkov. Nature of the Dirac gap modulation and surface magnetic interaction in axion antiferromagnetic topological insulator MnBi2Te4. *Sci Rep* **10**, 13226, doi:10.1038/s41598-020-70089-9 (2020).

[12] Przemyslaw Swatek, Yun Wu, Lin-Lin Wang, Kyungchan Lee, Benjamin Schrunk, Jiaqiang Yan & Adam Kaminski. Gapless Dirac surface states in the antiferromagnetic topological insulator MnBi2Te4. *Physical Review B* **101**, 161109, doi:10.1103/PhysRevB.101.161109 (2020).

[13] A. M. Shikin, D. A. Estyunin, N. L. Zaitsev, D. Glazkova, I. I. Klimovskikh, S. O. Filnov, A. G. Rybkin, E. F. Schwier, S. Kumar, A. Kimura, N. Mamedov, Z. Aliev, M. B. Babanly, K. Kokh, O. E. Tereshchenko, M. M. Otrokov, E. V. Chulkov, K. A. Zvezdin & A. K. Zvezdin. Sample-dependent Dirac-point gap in MnBi2Te4 and its response to applied surface charge: A combined photoemission and ab initio study. *Physical Review B* **104**, 115168, doi:10.1103/PhysRevB.104.115168 (2021).

[14] D. Zhang, M. Shi, T. Zhu, D. Xing, H. Zhang & J. Wang. Topological Axion States in the Magnetic Insulator MnBi2Te4 with the Quantized Magnetoelectric Effect. *Phys Rev Lett* **122**, 206401, doi:10.1103/PhysRevLett.122.206401 (2019).

[15] M. M. Otrokov, I. P. Rusinov, M. Blanco-Rey, M. Hoffmann, A. Y. Vyazovskaya, S. V. Eremeev, A. Ernst, P. M. Echenique, A. Arnau & E. V. Chulkov. Unique Thickness-Dependent Properties of the van der Waals Interlayer Antiferromagnet MnBi2Te4 Films. *Phys Rev Lett* **122**, 107202, doi:10.1103/PhysRevLett.122.107202 (2019).

[16] Jiaheng Li, Yang Li, Shiqiao Du, Zun Wang, Bing-Lin Gu, Shou-Cheng Zhang, Ke He, Wenhui Duan & Yong Xu. Intrinsic magnetic topological insulators in van der Waals layered MnBi2Te4-family materials. *Science Advances* **5**, eaaw5685, doi:10.1126/sciadv.aaw5685 (2019).

[17] Chaowei Hu, Anyuan Gao , Bryan Stephen Berggren , Hong Li, Rafa Kurleto, Dushyant Narayan, Ilija Zeljkovic, Dan Dessau, Suyang Xu, and Ni Ni. Growth, characterization, and Chern insulator state in MnBi2Te4 via the chemical vapor transport method. PHYSICAL REVIEW MATERIALS 5, 124206 (2021)

Current Activities of Research and Education on BL-5 (FY2022)

T. Yokoya[a,b], T. Wakita[a] and Y. Muraoka[a,b]

[a]*Research Institute for Interdisciplinary Science, Okayama University*
[b]*Research Laboratory for Surface Science, Okayama University, Okayama 700-8530, Japan*

Keywords: Photoemission spectroscopy, photoelectron emission microscopy

We present an overview of our resent research and educational activities on beamline 5 (BL5) in the fiscal year 2022. Our beamline has two experimental stations in a tandem way. The first station is equipped with an angle-resolved photoemission spectrometer (ARPES), a low energy electron diffraction (LEED) apparatus and an X-ray source. The hemispherical analyzer of ARPES spectrometer (HA54, VSW) has a mean radius of 50 mm and is mounted on a twin axis goniometer in ultra-high vacuum chamber. Using this goniometer, one can perform ARPES and photoelectron diffraction (PED) measurements. It is also possible to perform resonant photoemission spectroscopy (RPES) measurements by using photon energy tunability of synchrotron radiation with X-ray absorption spectroscopy (XAS) measurement. With the X-ray source (XR2E2, FISONS), we can perform an X-ray photoelectron spectroscopy (XPS) measurement for the chemical state analysis and the PED. At the second station, we have installed a photoelectron emission microscope (PEEM, 'PEEM III', Elmitec). PEEM provides a magnified image of lateral intensity distribution of photo-emitted electrons from a sample surface. The spatial resolutions are several ten nanometers with Hg lamp and a few micrometers with synchrotron radiation. The sample is transferred between the ARPES and the PEEM chamber in-situ, and one can perform measurements at both stations for the same sample.

In the recent researches on BL-5, we have studied the electronic structure of potassium doped aromatic molecule (K_x picene) [1], iron-based superconductor ($FeSe_xTe_{1-x}$) [2], transition metal di-oxide films such as VO_2 thin films which exhibits a first-order metal-to-insulator transition at 340 K [3], CrO_2 thin films which are known as a half-metallic material [4], TaO_2 film which is stabilized with a new technique developed in our group [5], and phase-separated TiO_2-VO_2 films on mica substrates. We have also studied the electronic structures of a high-quality boron-doped diamond film which shows a signature of the highest superconducting transition temperature of 25 K [6] and a high quality single crystal of $YbFe_2O_4$ which is one of multiferroic materials [7], by utilizing RPES at B *K*- and Fe $M_{2,3}$- edges, respectively. In addition, we have studied the sp^3 content in diamond-like carbon films by using photoemission spectroscopy in order to optimize the conditions to produce Q-carbon (quenched carbon) which is a newly discovered amorphous phase of carbon with several exotic properties [8]. In this fiscal year, we have performed PEEM and TEY measurements at BL5 in HiSOR for a B-doped carbon nano wall film on a Si substrate and a micro-droplet of solidified L-boronophenylalanine on a Si substrate in order to investigate microscopic chemical states of trace B atoms in them from fine structures in local- and wide-area-XAS spectra near B *K*-edge and to visualize B distributions on their surfaces.

Recently, we have prepared an auto-measurement system and an X-ray focusing capillary lens for photoemission holography (PEH). PEH is a method that has been greatly developed in Japan in recent years as a measurement method for elucidating the local structure of materials with an atomic resolution [9]. In particular, various results have been reported in the study of the three-dimensional atomic configurational structure around the dopants in crystals [10]. However, the opportunity to use state-of-the-art apparatuses (for example, DA30 analyzer and RFA of BL25SU at SPring-8) are limited. Although our photoelectron energy analyzer is an old model and it is difficult to separate and observe small shifts in core levels because of the energy resolution of 1-2 eV of the system, preliminary experiments on undoped materials can be carried out with our apparatus before the experiment using the latest ones. It can also be used for educational purposes such as experiencing photoelectron holography experiments and learning the analysis methods.

We have used the BL-5 for education activity as well, for example, practical education for undergraduate students of Okayama University. The students have an opportunity to study the synchrotron radiation mechanism and to experience XPS measurement which is very useful for the surface science research. We accepted more than 100 students from 2006 to 2012. From 2014, we have started to join the practical lecture for experiments using the beamline end stations in HiSOR for both graduate school students of Hiroshima and Okayama Universities. In 2018, we have had a new project for education under a Japan-Asia youth exchange program in science supported by Japan Science and Technology Agency (JST), "Sakura Exchange Program in Science". We have accepted six students from Changchun University of Science and Technology in China.

REFERENCES

1. H. Okazaki *et al*., *Phys. Rev* **82**, pp. 195114 (5 pages) (2010).
2. Y. Yoshida *et al*., *J. Phys. Soc. Jpn* **78**, pp. 034708 (4 pages) (2009).
3. K. Saeki *et al*., *Phys. Rev* **80**, pp. 125406 (5 pages) (2009).
4. Y. Muraoka *et al*., *MRS Proceedings* **1406** (2012).
5. Y. Muraoka *et al*., *Thin Solid Films* **599**, pp. 125-132 (2016).
6. H. Okazaki *et al*., *Appl. Phys. Lett* **106**, pp. 052601 (5 pages) (2015).
7. K. Fujiwara *et al*., *Trans. Mater. Res. Soc. Jpn.* **41**, pp. 139-142 (2016).
8. H. Yoshinaka *et al*., *Carbon.***167**, pp. 504-511 (2020).
9. T. Matsushita *et al*. *Europhys. Lett*. **71**, 597 (2005). *Phys. Status Solidi B* **255**, 1800091 (6 pages) (2018).
10. K. Hayashi, T. Matsushita, *SPring-8 Research Frontiers* **2020**, pp. 12 -15 (2021).

X-ray absorption spectroscopy of photodamaged polyimide film

○Osamu Takahashi[a,d] , Takuma Ohnishi[a,d], Ryosuke Yamamura[a,d], Eiichi Kobayashi[b], Kenta Kubo[c,d], Mayako Okazaki[c,d], Yuka Horikawa[c,d], Masaki Oura[d], and Hiroaki Yoshida[a,e]

[a]*Basic Chemistry Program, Graduate School of Advanced Science and Engineering, Hiroshima University*
[b]*Kyushu Synchrotron Light Research Center, 8-7 Yayoigaoka, Tosu, Saga 841-0005, Japan*
[c]*Department of Physics and Information Science, Yamaguchi University, Japan*
[d]*RIKEN SPring-8 Center, Kouto, Sayo-gun, Hyogo 679-5148, Japan*
[e]*Hiroshima Synchrotron Radiation Center, Hiroshima University, Kagamiyama, Higashi-Hiroshima, 739-0046, Japan*
Continue Here

Keywords: XAS, Polyimide, theoretical calculation

Polyimide, Capton, is a kind of organic polymers including imide bonds, and it has high electrical insulation and mechanical strength, and is used in a variety of applications such as insulating films. It is also known that it has gradually a damage due to light irradiation, but the mechanism is still controversial and the details are not well understood.

In the present study, photo-damaged mechanism is examined by visible light using X-ray absorption spectroscopy (XAS). Photo-damaged polyimide films for 24 – 96 hours are prepared in advance. Then XAS spectra are obtained XAS spectra at C, N, and O K-edges. XAS of polyimide film at the O K-edge is shown in Figure 1. Light irradiation for 48 hours or more shows broadening of the peak at 533 eV derived from the product oxidized by C-N bond cleavage. And by theoretical calculations using density functional theory, XAS spectra of monomer model and corresponding dissociated products are produced.

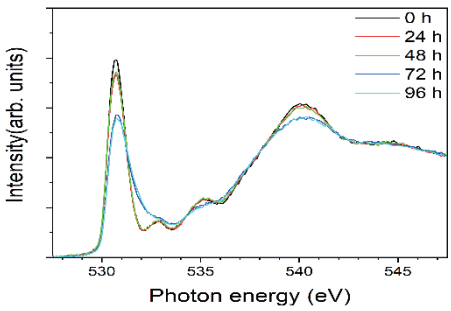

FIGURE 1. XAS spectra of polyimide film at O K-edge.

22BU001, 22BU002, 21BG014, 21BG015, 21AU001, 21AU007, 20AG023, 20AG024

BL-7, RIPES

Changes in Electronic States in Gd-TM metallic glasses Rejuvenated by Temperature Cycling

Shinya Hosokawa and Kentaro Kobayashi

Institute of Industrial Nanomaterials, Kumamoto University, Kumamoto 860-8555, Japan

Keywords: Metallic glasses, Rejuvenation effect, Temperature cycling, Electronic structures, Core levels

Rejuvenation in glasses is defined as an excitation to a higher energy state by an external stress, the opposite of the usual relaxation by thermal annealing. A rejuvenation effect by a temperature cycling in metallic glasses (MG) was recently reported by Ketov *et al*. on a $La_{55}Ni_{10}Al_{35}$ bulk MG [1]. They found such a rejuvenation effect by cycling between liquid N_2 and room temperatures in several macroscopic properties. According to their interpretation, the thermal expansion coefficient has a distribution over a glass sample if it is not elastically homogeneous. By repeated temperature changes, the different magnitudes of thermal expansion at different positions in a glass induces shearing forces, and as a result, a rejuvenation effect occurs in the glass. They called this 'Rejuvenation of metallic glasses by non-affine thermal strain' [1]. The validity of this picture is the subject of intensive debate.

Hufnagel reviewed thermal cycling rejuvenation effect, named as 'cryogenic rejuvenation', and suggested that non-affine deformation must be caused on an atomistic length scale [2]. The extent of the heterogeneity of glasses can be judged by the magnitude of so-called β-relaxation peak in dynamical mechanical analysis (DMA) spectra, and large peaks were detected in Gd-transition metal (TM) glasses by Yamasaki [3]. By referencing these ideas and results, we recently measured high energy x-ray diffraction (HEXRD) and anomalous x-ray scattering (AXS) on a $Gd_{65}Co_{35}$ metallic glass by comparing before and after the temperature cycling, and the structural data were analyzed by reverse Monte Carlo modeling [4]. Tiny but clear structural changes are observed by HEXRD in the nearest neighboring region of the real space pair distribution function. Partial structural information obtained by AXS reveals that slight movements of the Gd and Co atoms occur in the first- and second peaks in the nearest neighboring shells around the central Gd atom. We expect that electronic structures may be largely affected by these structural changes by the cryogenic rejuvenation.

In this series of experiments, we carried out photoemission and inverse-photoemission spectroscopies (PES and IPES) on $Gd_{65}TM_{35}$ (TM = Co and Ni) metallic glasses to clarify the rejuvenation effects in the valence- and conduction band densities of states (DOSs) in these glasses, respectively. Master $Gd_{65}TM_{35}$ ingots were manufactured by arc-melting a mixture of pure Gd and TM metals in an Ar atmosphere. The purities of Gd, Co, and Ni were 99.95, 99.999, and 99.999 at.%, respectively. Glassy foils with a thickness of about 20 μm and width of about 2 mm were prepared by melt spinning with a single Cu roll in a pure Ar atmosphere. The concentration was confirmed to be within 0.5 wt.% of the nominal values by electron-probe micro-analysis. A thermal cycling treatment was made between liquid N_2 and room temperatures 40 times, and all the experiments were performed for the same sample foils before and after the above temperature cycling.

The PES spectra were measured using a spectrometer installed at BL-7 of Hiroshima Synchrotron Radiation Center (HSRC). Ultraviolet photons generated from a compact electron-storage ring (HiSOR) were monochromatized with a Dragon-type monochromator, covering the incident photon energy, $h\nu$, values from 20 to 450 eV. A PES spectrometer with a hemispherical photoelectron energy-analyzer (GAMMA-DATA, SCI- ENTA SES2002) attached to the analyzer chamber under the ultrahigh vacuum below 1×10^{-8} Pa at the end-station of BL-7, was used for the PES experiments. The overall energy resolution, ΔE, of the spectrometer was about 0.1-0.5 eV depending on the $h\nu$ values of 20-450 eV. All the PES spectra were collected at room temperature. Clean surfaces were in situ obtained by sputtering the samples with Ar^+ ions in a sample preparation chamber with the base pressure below 1×10^{-8} Pa. The energies of all spectra were defined with respect to the Fermi energy, E_F, of the sample or a freshly evaporated Au film.

The IPES experiments were carried out at the resonant IPES spectroscopy (RIPES) station in the HSRC. The self- developed IPES spectrometer is equipped with a low-energy electron gun, a non-periodic spherical grating, and a one-dimensional photon detector. The total energy resolution was ~0.5 eV at the electron gun energy E_k of 50 eV. The energy of the IPES spectra is referred to E_F, determined from the Fermi edge of the IPES spectra of a Au film. All the IPES experiments were also carried out at room temperature. Clean surfaces were in situ obtained by scraping the samples with a diamond filer in a sample preparation chamber attached with the analyzer one, both of which were kept under ultrahigh vacuum below 1×10^{-8} Pa.

Left panel of Fig. 1 shows the valence-band PES spectra on the $Gd_{65}Co_{35}$ glass at $h\nu$ of 40-230 eV before (blue curves) and after (red curves) the cryogenic rejuvenation. The spectral features drastically change with varying $h\nu$. Right panel of Fig. 1 shows the $h\nu$ dependence of photoionization cross-sections of Gd 4*f*, 5*d*, and 6*s*, and Co 3*d* and 4*s* electrons. By taking this figure into account, the peaks in the ranges around -5 and -8 eV are mainly composed of the Co 3*d* and Gd 4*f* electrons, respectively. By the cryogenic rejuvenation, only the Co 3*d* peak largely decreases.

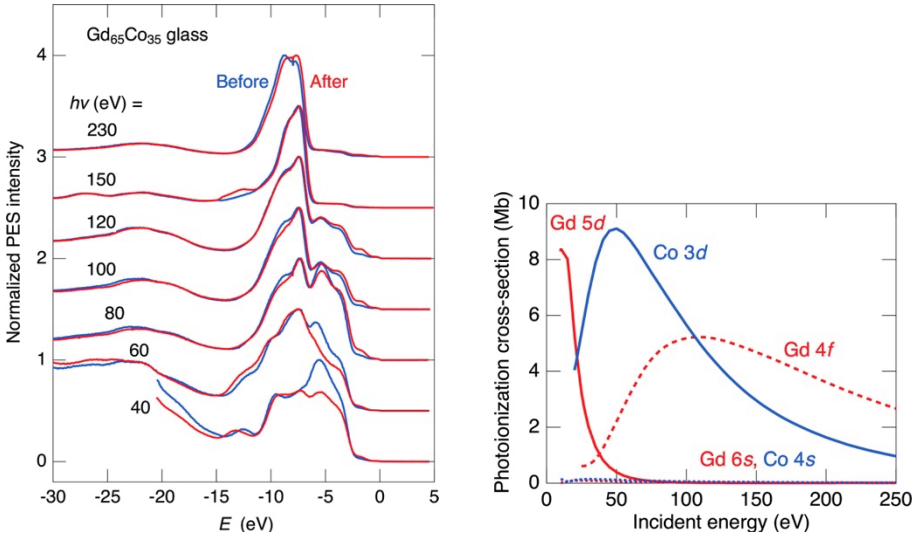

FIGURE 1. (Left) Valence-band PES spectra on $Gd_{65}Co_{35}$ glass before (blue curves) and after (red curves) the cryogenic rejuvenation. (Right) Incident photon energy dependence of the photoionization cross-sections of Gd 4*f*, 5*d*, and 6*s*, and Co 3*d* and 4*s* electrons.

Left and right panels of Fig. 2 show the Gd 4*d* and Co 3*p* core-level PES spectra on the $Gd_{65}Co_{35}$ glass measured at $h\nu$ = 230 eV. By the temperature cycling, the peak in the Gd 4*d* spectrum at about -142 eV slightly shifts towards the shallower energy direction, while the peak in the Co 3*p* spectrum at about -60 eV looks mostly unchanged, suggesting the chemical mature of the Gd atoms may be slightly changed reflecting the structure changes by the rejuvenation.

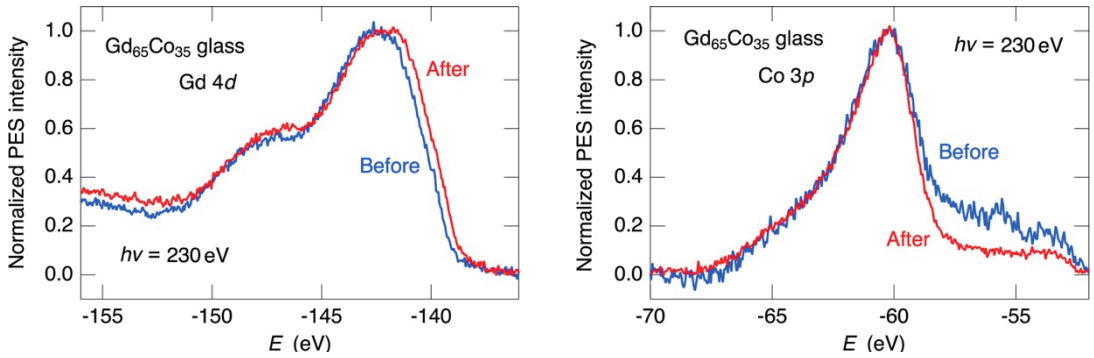

FIGURE 2. Gd 4*d* (left) and Co 3*p* (right) core-level PES spectra on $Gd_{65}Co_{35}$ glass before (blue curves) and after (red curves) the cryogenic rejuvenation.

Left and right panels of Fig. 3 show the conduction-band IPES spectra on the $Gd_{65}Co_{35}$ and $Gd_{65}Ni_{35}$ glasses before (blue curves) and after (red curves) the cryogenic rejuvenation, respectively. As clearly seen in the figures, the empty-state spectra of $Gd_{65}Co_{35}$ and $Gd_{65}Ni_{35}$ glasses resemble each other. The prominent peak at about 7 eV shifts to about 5.5 eV and becomes sharper and higher in the height. Since the spectra of these glasses are very similar, the origin of this peak may be the Gd atoms.

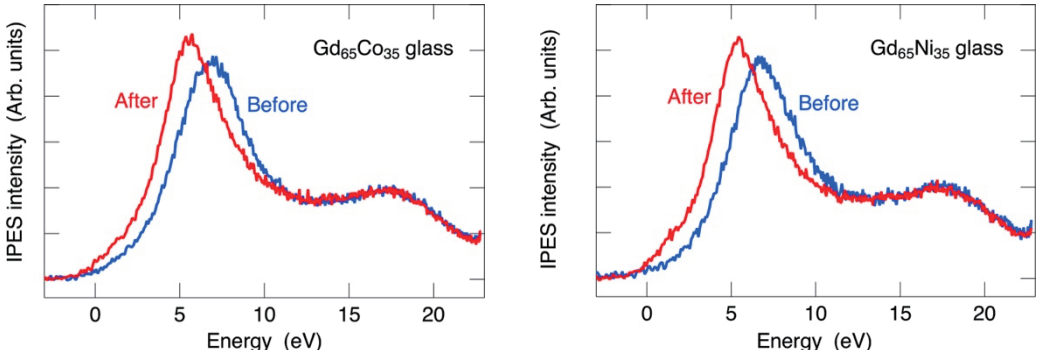

FIGURE 3. Conduction-band IPES spectra on $Gd_{65}Co_{35}$ (left) and $Gd_{65}Ni_{35}$ (right) glasses before (blue curves) and after (red curves) the cryogenic rejuvenation.

In addition to these works, we measured soft x-ray absorption and emission spectroscopies near the Co and Ni 2*p*-3*d* resonances, and the 3*d* partial DOS are obtained. The results are under analyzing. Moreover, an *ab-initio* molecular dynamics simulation is planned to obtain further on the atomic and electronic changes by the cryogenic rejuvenation on the Gd-TM glasses.

This work was supported by the Japan Society for the Promotion of Science (JSPS) Grant-in-Aid for Transformative Research Areas (A) 'Hyper-Ordered Structures Science' (Nos. 20H05878 and 21H05569), that for Scientific Research (C) (No. 22K12662), the Japan Science and Technology Agency (JST) CREST (No. JP-MJCR1861).

REFERENCES

1. S. V. Ketov, Y. H. Sun, S. Nachum, Z. Lu, A. Checchi, A. R. Beraldin, H. Y. Bai, W. H. Wang, D. V. Louzguine-Luzgin, M. A. Carpenter, and A. L. Greer, *Nature* 524, 200-203 (2015).
2. T. C. Hufnagel, *Nature Mater.* **14**, 867-868 (2015).
3. Y. Yamazaki, *Doctoral thesis* (Tohoku University, 2016).
4. S. Hosokawa, J. R. Stellhorn, L. Pusztai, Y. Yamazaki, J. Jiang, H. Kato, T. Hayashi, T. Ichitsubo, E. Magome, N. Blanc, N. Boudet, K. Ohara, S. Tsutsui, H. Uchiyama, and A. Q. R. Baron, *Nature Commun.*, submitted.

Electronic structure of Heusler-type $Fe_2V_{1-x}Ti_xAl$ single-crystal studied by X-ray photoelectron spectroscopy

Kyoya Kosemura[a] and Hidetoshi Miyazaki[a, b]

[a]*Department of Physical Science and Engineering, Nagoya Institute of Technology, Gokiso-cho, Showa-ku, Nagoya 466-8555, Japan*
[b]*Creative Engineering Program, Nagoya Institute of Technology, Gokiso-cho, Showa-ku, Nagoya 466-8555, Japan*

Keywords: Heusler-type Fe_2VAl alloy, Electronic structure, thermoelectric property, oxidation resistance, Photoelectron spectroscopy.

Heusler-type Fe_2VAl-based alloys have a sharp pseudogap near the Fermi level, and the thermoelectric performance can be improved by optimizing the Fermi level through fourth element substitution or non-stoichiometric composition [1][2]. This material is also attracting attention as a high-strength material for high-temperature applications because it is almost impervious to oxidation at high temperatures. In order to clarify the mechanism of thermoelectric performance enhancement and high oxidation resistance, it is important to directly observe the electronic structure of this materials. In this experiment, photoelectron spectroscopy measurements at HiSOR BL7 were performed mainly on samples that had undergone surface treatment at various annealing temperatures to elucidate the mechanism of high oxidation resistance at high temperatures.

A single crystal sample was prepared by the Choklarsky method from a polycrystalline ingot with a target composition of $Fe_2V_{0.94}Ti_{0.06}Al$ weighed with 0.65 at% more Al composition. The crystal growth orientation was then examined by the back reflection Laue method. To investigate the composition of the prepared single-crystal samples, Seebeck coefficient and electrical resistivity were measured and the composition was analyzed by X-ray fluorescence, and compared with the values of the polycrystal samples of the target composition to determine the samples for photoelectron spectroscopy measurements. Figure 1 shows temperature-dependence of Seebeck coefficients of poly- and single-crystalline Heusler-type $Fe_2V_{1-x}Ti_xAl$ alloys. The behavior of Seebeck coefficient versus temperature for the single-crystal and polycrystal samples was consistent, indicating identical composition. Photoelectron spectroscopy measurements with photon energy of 200 eV were performed at BL-7 of HiSOR.

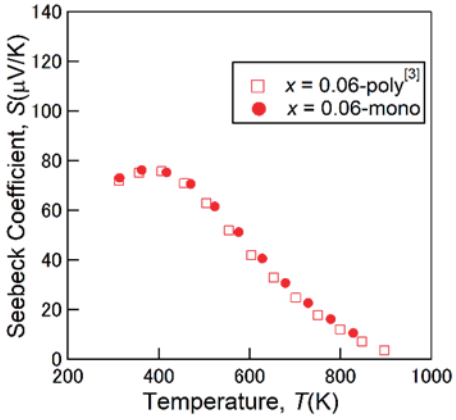

FIGURE 1. Temperature dependence of Seebeck coefficients of Heusler-type $Fe_2V_{1-x}Ti_xAl$ poly- and single-crystalline.

Figure 2 shows the results of photoelectron spectroscopy measurements performed on single-crystal $Fe_2V_{0.94}Ti_{0.06}Al$ while annealing. Annealing conditions were set to 800, 1000, and 1000 °C over. In all annealing conditions, peaks at binding energies, E_B, 119 and 76 eV were found to be caused by Al 2*s* and Al 2*p* states. As the annealing temperature was increased, the intensity of the peaks of Al 2*s* and Al 2*p* states increased, while the peaks around E_B = 84 eV and 100 eV decreased. This change in peak intensity can be attributed to the formation of a strong oxide film on the surface by annealing. Some peaks that cannot be attributed to any constituent elements were observed, but these are considered to be Auger peaks or peaks due to higher-order light that may have penetrated into the material due to the characteristics of the beamline used in this study. In the annealed single crystal $Fe_2V_{0.94}Ti_{0.06}Al$, the Al oxide peak was stronger, but the Al metal peak due to the bulk was also observed at the same intensity. This indicates that a thin oxide film was formed on the sample surface. The sample was left in the air for two months, and the slow progress of oxidation suggested the possibility of improving the oxidation resistance performance of the sample.

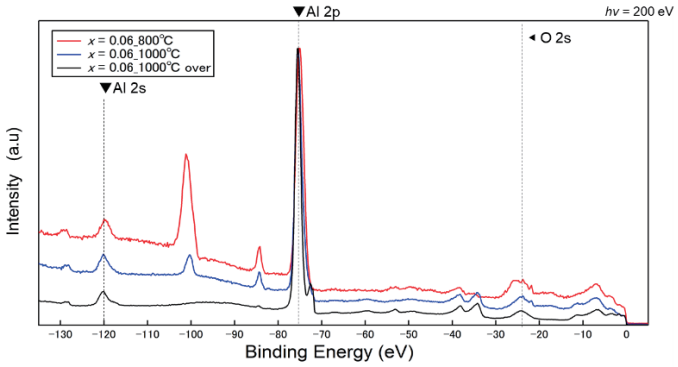

FIGURE 2. Annealing temperature dependence of photoelectron spectra of Heusler-type $Fe_2V_{1-x}Ti_xAl$ single crystal.

REFERENCES

1. H. Matsuura, Y. Nishino, U. Mizutani and S. Asano, J. Japan Inst. Metals **66**, 767-771 (2002).
2. H. Miyazaki, S. Tanaka, N. Ide, K. Soda and Y. Nishino, Mater. Res. Express **1**, 015901 (2014).
3. Y. Nishino, S. Kamizono, H. Miyazaki and K. Kimura, AIP Advances **9**, 125003 (2019).

Photoelectron spectroscopy of beta-tungsten thin-films

H.T. Lee[a] and H. Sato[b]

[a]*Graduate School of Engineering, Osaka University, Suita 565-0871, Japan*
[b] *Hiroshima Synchrotron Radiation Center, Hiroshima University, Higashi-Hiroshima 739-0046, Japan*

Keywords: Electronic structure, Photoelectron spectroscopy, Spintronic devices, Thin films

β-tungsten (β-W)/ferromagnetic thin film heterostructures have exhibited large room temperature spin orbit torques (SOT) [1], making them attractive for spintronics. The origin of the large SOT is still debated (bulk or interface effects). On the one hand, theoretical studies of perfect β-W crystals have shown that large spin conductivities are intrinsic to the A15 structure [2,3]. Such phenomena arise from several unprotected crossings near the Fermi level which results in a net large spin berry curvature. On the other hand, it has been shown experimentally that the measured large spin Hall angles are insensitive to oxygen-doping levels [4], suggesting that the SOT originates primarily from the interface rather than from bulk properties. To date, no work has experimentally examined the electronic density of states in β-W thin films and the effects of oxygen incorporation. In this work, we build upon our previous work in synthesizing high quality β-W thin films [5] to study the effect of oxygen incorporation on the electronic properties of β-W thin films.

Figure 1 shows the core and valence band spectra of β-W thin films containing two different oxygen concentrations (<1 and ~10 at.%) at photon energy of 120 eV following 80 s Ar-sputtering. The average oxygen concentrations in the interior of the films were determined from O 1*s*/W 4*f* ratios determined from separate sputter-XPS experiments. An increase in oxygen concentration results in noticeable broadening of the W 4*f* core spectra, resulting in distortion at both the leading and trailing edges. Correspondingly, the valence band spectra show a broadening of the Fermi edge, as well as the shift of the peak closest to the Fermi edge to lower energies. The second peak at -6.5 eV remains largely unshifted, while the third peak at -12.5 eV is no longer visible.

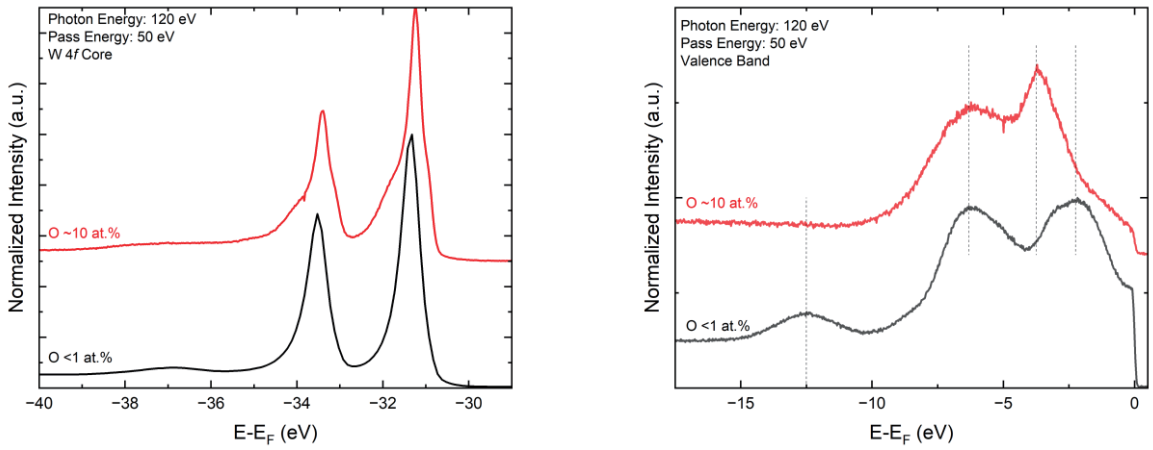

FIGURE 1. Comparison of core and valence band spectra of β-W thin films containing different Oxygen concentrations.

Figure 2 shows the core and valence band spectra of both α- and β-W thin films with ~10 at.% oxygen at photon energy of 400 eV. Qualitatively, there are no significant differences between the core and valence spectra of α- and β-W thin films. Although the core band spectra shows broadening, the W 4*f* doublet peak is located at 31.29 eV with 2.18 eV width between the doublet for both α- and β-W thin films. This is in excellent agreement with the location of metallic W located at 31.3±0.2 eV and 2.18 eV from the average of

values in the NIST database. A 0.1 eV shift to higher energies in the W 4*f* peak maximums are observed for β-W. This shift could be due to the higher coordination number of the W atoms in β-W (12 or 14) in comparison to α-W (8), but may also arise from effects of defects introduced either during synthesis or during Ar sputter cleaning. At this photon energy the cross-section of O 2*p* is lower than O 2*s*, in contrast to it being higher at photon energy of 120 eV. From the valence band spectra, it is clear that the second peak at -6.5 eV is diminished in comparison to Figure 1, suggesting that the second peak is a feature of the O 2*p*.

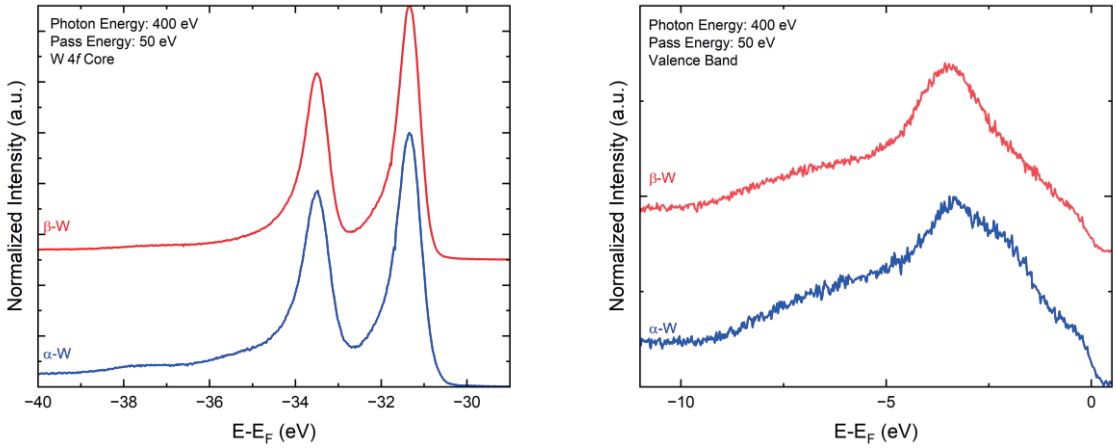

FIGURE 2. Comparison of core and valence band spectra of α- and β-W thin films with ~10 at.% oxygen.

REFERENCES

1. C-F. Pai et al., *Appl. Phys. Letters* **101**, 122404 (2012).
2. X. Sui et al., *Phys. Rev. B* **96**, 241105 (2017).
3. E. Derunova et al., *Sci. Adv.* **5**, eaav8575 (2019).
4. K. Demasius et al., *Nat. Comm.*, **7**, 10644 (2016).
5. A. Nagakubo, H.T. Lee et al., *Appl. Phys. Letters* **116**, 021901 (2020).

Attempt of edge states observation on the surface different from the cleavage planes in $TlBiSe_2$

K. Miyamoto[a*], T. Onogi[b], H. Sato[a] and T. Okuda[a]

[b]*Department of Science, Hiroshima University 1-3-1 Kagamiyama, Higashi-Hiroshima 739-8526, Japan*
[a]*Hiroshima Synchrotron Radiation Center, Hiroshima University, 2-313 Kagamiyama, Higashi-Hiroshima 739-0046, Japan*

Keywords: Topological surface state, strong topological insulator

Recently, topological insulators have attracted attention as a candidate for the useful spintronics materials[1]. Three-dimensional topological insulators are insulators in the bulk and have spin-polarized metallic electronic states (edge states) on the surface. In general, there are two types of topological insulators such as weak topological insulators and strong topological insulators. The weak topological insulators possess their edge state only in certain surface orientations as has been observed very recently [2]. On the other hand, surfaces with any orientation can have edge state in the strong topological insulators. Actually, many materials like Bi_2Se_3, Bi_2Te_3, and $TlBiSe_2$ were predicted as strong topological insulators by band calculations and their edge states have been discovered by angle-resolved photoemission spectroscopy (ARPES) measurement [3,4]. However, so far, observation of edge states has been limited only to cleaved planes due to the difficulty of obtaining clean surfaces on non-cleaved planes, and clear experimental evidence for strong topological insulators is lacking.

In this study, we attempted to observe the edge states of $TlBiSe_2$ which is considered to be a strong topological insulator with the $(11\bar{2})$ surface plane which is different from the cleaved (111) surface, with the use of ARPES measurements. The clean $(11\bar{2})$ surface is prepared by mechanical polishing followed by repeated cycles of Ar-ion bombardment (1.5 keV) and annealing at 700 K. Cleanness of the surface was checked by Auger electron spectroscopy and by low energy electron diffraction patterns with super-structure as shown in Fig.1. ARPES measurement was performed at bending magnet beamline BL-7 in Hiroshima Synchrotron Radiation Center. The sample temperature was set at 50K.

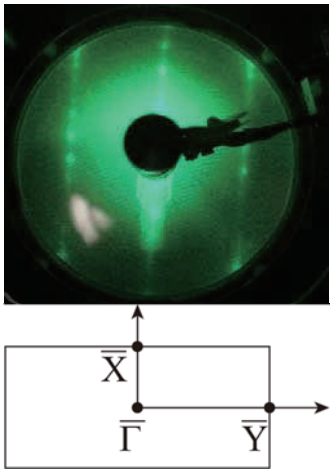

Fig.1 LEED patterns and surface Brillouin zone

Figure 2 shows the observed energy band dispersions taken at photon energies (hν) of 70, 60, and 50eV along $\overline{\Gamma Y}$ symmetry line. In Fig. 2(a), a band dispersion is observed near Fermi energy, in which the band top is located at E_B= 0.25 eV at $\bar{Y}$ point. Here, the peak positions of the band obtained by the fitting of peak positions in the momentum distribution curves (MDCs)

by the Voigt function are indicated by white lines.

In order to determine whether the observed band is a surface (i.e. edge state) or a bulk electronic state, the photon energy dependence in ARPES measurements were performed as in Figs. 2(b) and 2(c). As a result, the observed bands gradually shift toward the $\bar{\Gamma}$ point as the photon energy decreases. Therefore, we conclude that the observed band near E_F is not the edge state but the bulk state.

In summary, we have tried to measure the electronic structure of $TlBiSe_2$ with the $(11\bar{2})$ surface. However, the edge state unique to the strong topological insulator were not found, but the bulk-like bands are observed. The reason why the surface state could not be observed is not obvious but might be due to the roughness of the surface or some surface contamination which is seen in the ARPES spectra as a small peak at around E_B = 6eV. As these consequences, the photoemission intensities of edge states might be too small to observe. Further experiment with better surface quality is desirable to see the clear evidence of strong topological insulator.

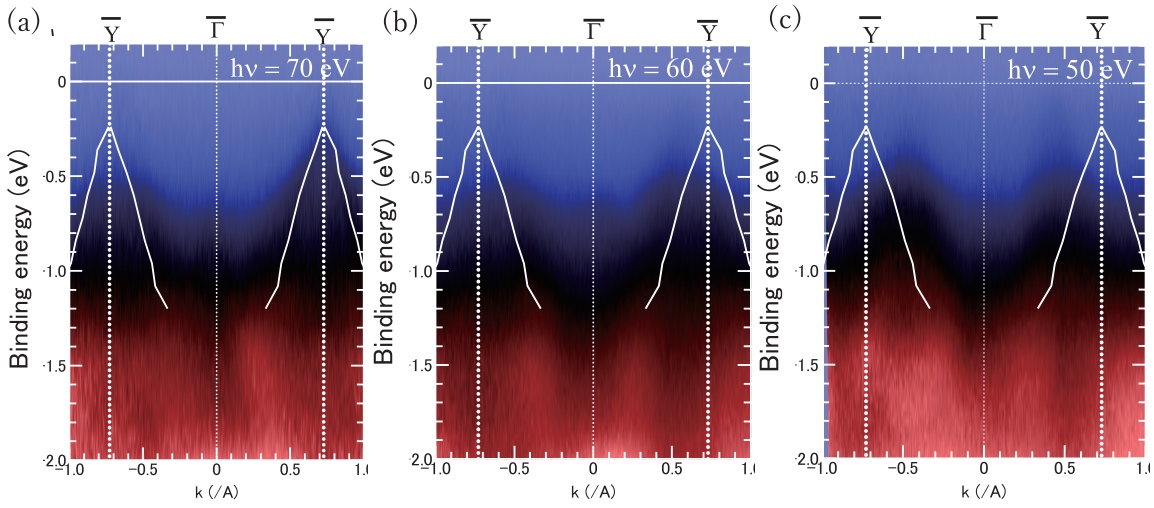

Fig.2 Photon energy dependence of the band dispersion obtained by ARPES. White solid lines indicate the peak position estimated from the momentum distribution curves (MDCs) taken at hν = 70 eV. These peak positions are obtained by fitting of MDCs at each binding energy with Voigt function.

REFERENCES

1. M. Z. Hasan and C. L. Kane, *Rev. Mod. Phys.* **82**, 3045 (2010).
2. R. Noguchi et al., *Nature* **566**, 518-522 (2019).
3. K. Kuroda et al., *Phys. Rev. Lett.* **105**, 076802 (2010).
4. K. Kuroda et al., *Phys. Rev. Lett.* **105**, 146801 (2010)./T. Sato et al., *Phys. Rev. Lett.* **105**, 136802 (2010).

Investigating the possibility of creating a “pure” p-type Bi_2Se_3

Yuki Higuchi[a], Ryota Itaya[a], Mito Tomita[a], Harutaka Saito[b], Katsuhiro Suzuki[b], Hitoshi Sato[c], Kazunori Sato[b,d], and Kazuyuki Sakamoto[a,d]

[a] *Department of Applied Physics, Osaka University, Osaka 565-0871, Japan*
[b] *Division of Materials and Manufacturing Science, Osaka University, Osaka 565-0871, Japan*
[c] *Hiroshima Synchrotron Radiation Center, Hiroshima University, Higashi-Hiroshima 739-0046, Japan*
[d] *Spintronics Research Network Division, OTRI, Osaka University, Osaka 565-0871, Japan*

Keywords: Topological insulator, Bi_2Se_3, ARPES, QSGW calculation

Three-dimensional topological insulators (TIs), which hold spin-polarized Dirac cone type metallic bands on the surface while the bulk is insulating, are promising materials to realize next-generation spintronics devices. For example, controlling the Fermi level by, *e.g.,* charge doping, and making both n-type and p-type from a single TI sample will allow to create p-n topological junction [1-4], a device that has a great possibility to solve the problem of processing the explosive volume of information, which cannot be solved by the existing electronics technology based solely on the charge degrees of freedom. Bi_2Se_3 is a typical n-type TI whose bulk valence band maxima (BVBM) was predicted to located close to the Dirac point (DP) both theoretically and experimentally [5-8]. This means that even by doping the sample and tuning the Fermi level below the DP, it is impossible to create a “pure” p-type Bi_2Se_3, because the bulk band crosses the Fermi level simultaneously. This situation makes the spin-polarized surface electrons diffusing into the bulk, and therefore difficult to generate a highly efficient spin current in practical applications.

In this study, we performed state-of-the-art ARPES measurements and DFT calculations to obtain precise information on the bulk band behavior to have a proper understanding on the electronic structure of Bi_2Se_3, and to discuss the feasibility of this TI for spintronics devices. ARPES measurements were performed at the beamline BL-7 of HiSOR. The bulk band along the $\bar{\Gamma}-\bar{\mathrm{M}}$ direction, the direction where the BVBM was predicted to be above the DP, was measured using photon energies ($h\nu$) from 33 eV to 89 eV. This $h\nu$ range covers more than a single Brillouin zone along the $k_\perp$ direction. Fig. 1(a) shows the band structure obtained at $k_\perp = 4.10\ \text{Å}^{-1}$ and Figs. 1(b)-(d) are the $k_\perp$-dependent EDCs measured at different $k_\parallel$. The band structure in Fig. 1(a) shows that the BVBM is located at the $\bar{\Gamma}$ point and below the DP, and a saddle-like-valence band (SVB) to be present along the $\bar{\Gamma}-\bar{\mathrm{M}}$ direction. Furthermore, the EDCs in Figs. 1(b)-(d) show that the BVMBs are located below the DP throughout the entire 3D Brillouin zone, and the SVB to show a $k_\perp$ dependence. In order to confirm these experimental results, we have performed DFT calculations using the Quasiparticle Self Consistent GW (QSGW) [9-11], a method that has the property of showing the band gap more accurately than the DFT calculations used in former studies. Two types of projected bulk band are shown in Fig. 2 (a) and(b). The theoretically obtained results using QSGW indicates the BVBM to be located at the Γ point, and therefore strongly support our experimental results. The present results also suggest that it is possible to make a “pure” p-type Bi_2Se_3 by hole-doping, and therefore the possibility of using this TI as a material to realize novel spintronics devices.

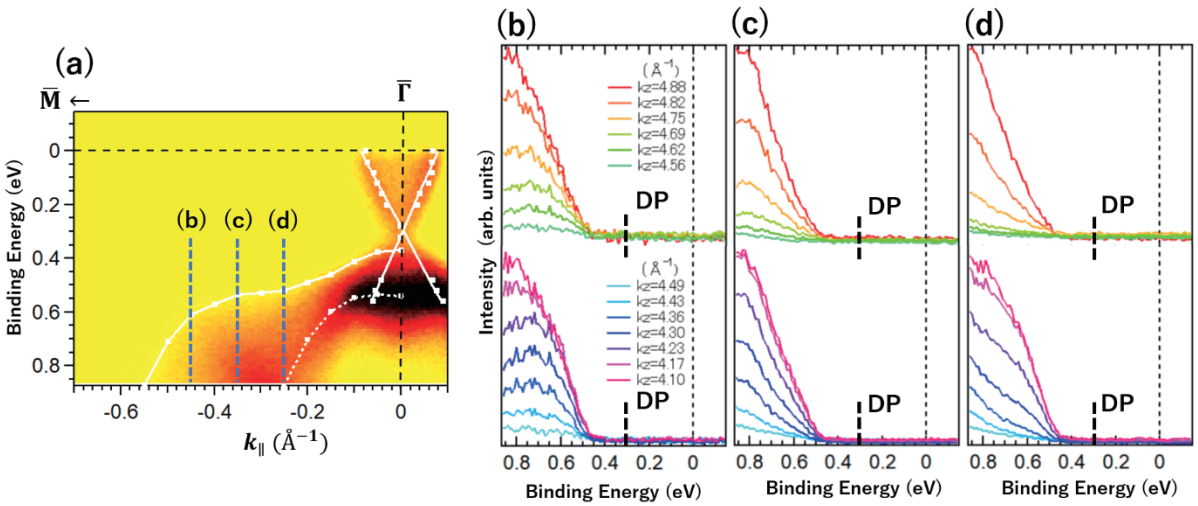

Figure 1. (a) Band structure of Bi_2Se_3 along $\bar{\Gamma}-\bar{M}$ at $k_\perp = 4.10$ Å^{-1}, and (b)-(d) $k_\perp$-dependent EDCs at different $k_\parallel$. $k_\perp = -0.45$ Å^{-1} in (b), -0.35 Å^{-1} in (c), and -0.25 Å^{-1} in (d). The range of $k_\perp$ is larger than that of single Brillouin zone.

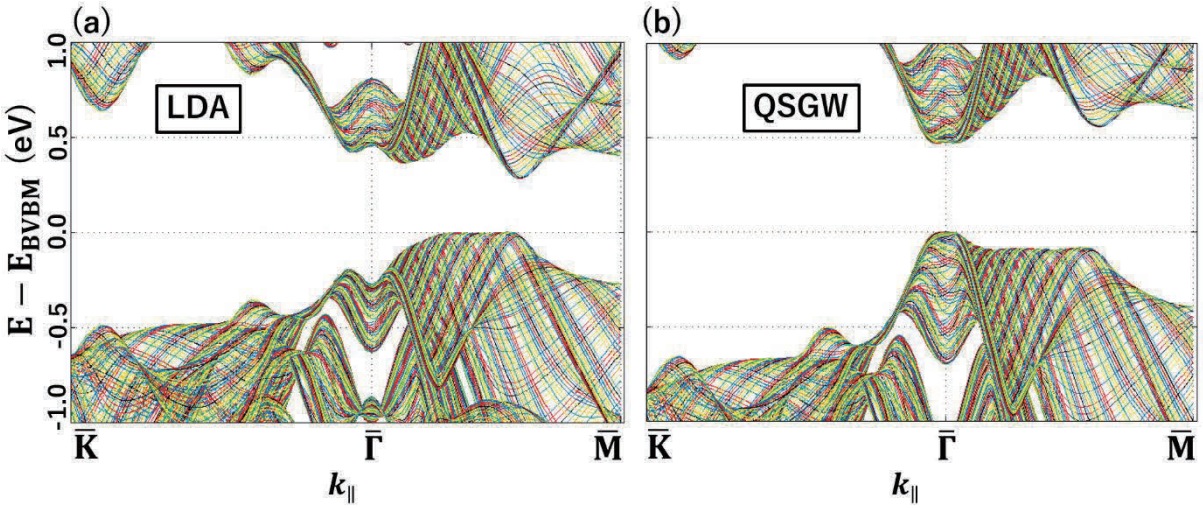

Figure 2. Theoretical projected bulk band structure along the $\bar{K}-\bar{\Gamma}-\bar{M}$ direction of the 2D Brillouin zone obtained using (a) LDA and (b) QSGW.

REFERENCES

1. J.-L. Mi, M. Bremholm, M. Bianchi, K. Borup, S. Johnsen, M. Søndergaard, D. Guan, R. C. Hatch, P. Hofmann, B. B. Iversen, *Adv. Mater.* **25**, 889 (2013).
2. N. H. Tu, Y. Tanabe, Y. Satake, K. K. Huynh, K. Tanigaki, *Nat. Commun.* **7**, 13763 (2016).
3. S. H. Kim, H.-H. Jin, B. W. Kho, B.-G. Park, F. Liu, J. S. Kim, and H. W. Yeom, *ACS Nano* **11**, 9671 (2017).
4. K. Sakamoto, H. Ishikawa, T. Wake, C. Ishimoto, J. Fujii, H. Bentmann, M. Ohtaka, K. Kuroda, N. Inoue, T. Hattori, T. Miyamachi, F. Komori, I. Yamamoto, C. Fan, P. Krueger, H. Ota, F. Matsui, F. Reinert, J. Avila, and M. C. Asensio, *Nano Lett.* **21**, 4415 (2021).
5. H. Chang, C.-X. Liu, X.-L. Qi, X. Dai, Z. Fang, and S.-C. Zhang, *Nature Phys.* **5**, 438 (2009).
6. Y. Xia, D. Qian, D. Hsieh, L. Wray, A. Pal, H. Lin, A. Bansil, D. Grauer, Y. S. Hor, R. J. Cava and M. Z. Hasan, *Nature Phys.* **5**, 398 (2009).
7. S. Kim, M. Ye, K. Kuroda, Y. Yamada, E. E. Krasovskii, E. V. Chulkov, K. Miyamoto, M. Nakatake, T. Okuda, Y. Ueda, K. Shimada, H. Namatame, M. Taniguchi, and A. Kimura, *Phys. Rev. Lett.* **107**, 056803(2011).
8. O. V. Yazyev, J. E. Moore, and S. G. Louie, *Phys. Rev. Lett.* **105**, 266806(2010).
9. T. Kotani, M. v. Schilfgaarde and S. V. Faleev, *Phys. Rev. B* **76**, 165106 (2007).
10. I. A. Nechaev, R. C. Hatch, M. Bianchi, D. Guan, C. Friedrich, I. Aguilera, J. L. Mi, B. B. Iversen, S. Blugel, Ph. Hofmann, and E. V. Chulkov, *Phys. Rev. B* **87**, 121111(R) (2013).
11. I. Aguilera, C. Friedrich, and S. Blügel, *Phys. Rev. B* **100**, 155147(2019).

Kondo-like peak in the photoemission spectra of quadruple perovskite oxides $SrCu_3Ru_4O_{12}$

Hiroaki Anzai[a], Yasuaki Kikuchi[a], Yuta Kato[a], Hitoshi Sato[b], Masashi Arita[b], Ikuya Yamada[a], and Atsushi Hariki[a]

[a] *Graduate School of Engineering, Osaka Prefecture University, Sakai 599-8531, Japan*
[b] *Hiroshima Synchrotron Radiation Center, Hiroshima University, Higashi-Hiroshima 739-0046, Japan*

Keywords: Kondo effect, *A*-site-ordered perovskite oxide, photoemission spectroscopy.

The quadruple perovskite oxide system $ACu_3Ru_4O_{12}$ provides a unique opportunity for studying a *d*-electron heavy-mass behavior. The electron specific heat coefficient of the A = Ca compound is estimated to be $\gamma \sim 84$ mJ/(mol·K^2), indicating a heavy effective mass of *d* electrons [1]. Moreover, the magnetic susceptibility χ exhibits a broad peak at $T \sim 190$ K [1]. This temperature dependence is quite similar to $\chi(T)$ for $CeSn_3$, which is a classical 4*f* electron heavy-fermion material [2]. The previous studies by photoemission spectroscopy have revealed that the hybridization between the localized Cu 3*d* electrons and the itinerant Ru 4*d* electrons is relevance to the emergence of the resonance-like peak near E_F [3,4]. Moreover, the first-principles calculation suggests that both Ru-O-Ru and Ru-O-Cu networks contribute to the conducting behavior [5]. Therefore, the band hybridization near E_F must be taken into account to interpret the mass enhancement of A = Ca. We recently synthesized a new compound $SrCu_3Ru_4O_{12}$ under high pressure. The ionic radius of Sr^{2+} is larger than that of Ca^{2+}, and thus the lattice expansion occurs with Sr substitution. The change in the hybridization strength will provide a new insight that can detect the dominant mechanism responsible for the *d*-electron heavy-mass behavior.

Here, we report a photoemission spectroscopy study on the quadruple perovskite oxides $SrCu_3Ru_4O_{12}$. The experiments were performed at BL-7 and BL-9A of Hiroshima Synchrotron Radiation Center. The photoemission data were collected with the photon energy of $h\nu = 16$ eV. The energy resolution was set to 13 meV. The samples were cleaved *in situ* and kept under an ultrahigh vacuum of 6.0×10^{-9} Pa during the measurements.

Figure 1(a) shows the photoemission spectra at $T = 10$ K for A = Sr samples. Two peaks are clearly observed at $|\omega| \sim 20$ (labeled α) and 80 meV (labeled β). We note that the shapes of the peak α and β are sharper than

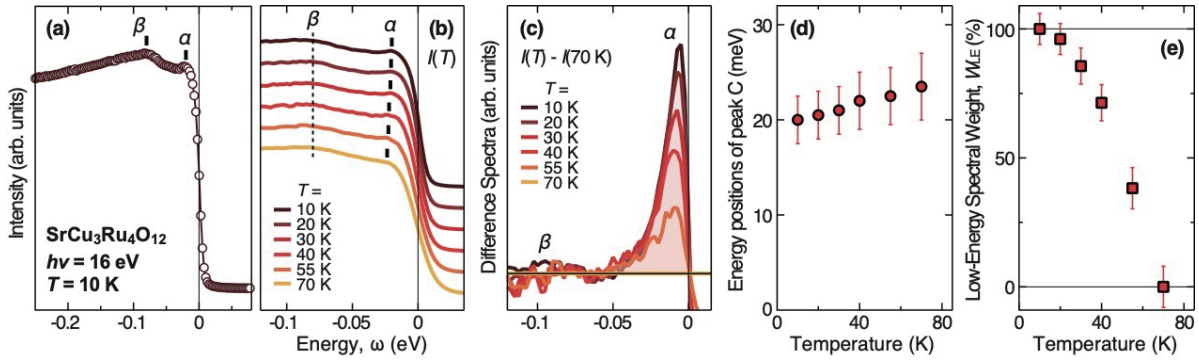

Figure 1. (a) Photoemission spectra of $SrCu_3Ru_4O_{12}$ measured at $T = 10$ K using $h\nu = 16$ eV photons. The vertical bars indicate the energy positions of the peak α and β. (b) Temperature dependence of the photoemission spectra near E_F. The black bars and dashed line denote the energy positions of the peak α and β, respectively. (c) Difference spectra obtained by subtracting the intensity at $T = 70$ K from that at each temperature, $I(T) - I(70\text{ K})$. The colored area indicates the spectral weight at low-energy region of $0 < |\omega| < 0.06$ eV. (d) Energy positions of the peak α as a function of temperature. (e) Temperature dependence of the low-energy spectral weight W_{LE}, which is determined by integrating the intensity over the energy window of the colored area in the difference spectra of (c). The weight is plotted as a percentage of the total weight at $T = 10$ K. The error bars are derived from statistics and reflected by noise in the data.

previously reported experiments on A = Ca [3,4]. The temperature dependence of the spectra is shown with vertical offsets in Fig. 1(b), which reveals a temperature evolution of the peak α between 10 and 70 K. In contrast, peak β is insensitive to temperature, implying a different origin to the peak α. We determined the energy of the peak α and plotted them as red circles in Fig. 1(d). The energy decreases gradually with decreasing temperature.

To quantified the intensity of the peak α, we extracted the difference spectra by subtracting the intensity at T = 70 K from that at each temperature, $I(T) - I(70\ \mathrm{K})$. This method effectively removes the background contribution from the photoemission spectra [6]. As shown by the difference spectra in Fig. 1(c), we obtained a clear view of the temperature evolution of the peak α. The spectral weight in the low-energy region W_{LE} was determined by integrating the intensity of the difference spectra in the energy window of $0 < |\omega| < 0.06$ eV. The colored area of the difference spectra in Fig. 1(d) corresponds to the low-energy spectral weight W_{LE}. Figure 1(e) shows the temperature dependence of W_{LE} as a percentage of the total weight at T = 10 K. With decreasing temperature, W_{LE} rapidly increases.

The 4*f* peak near E_{F} in the photoemission spectra of Yb-based heavy-fermion compounds exhibits a similar temperature-dependent evolution and is assigned to the Kondo resonance peak in accordance with the single impurity Kondo or Anderson model description [7]. This similarity on the A = Sr compounds implies that the temperature-dependent changes in the peak α are derived from the hybridization between the itinerant electrons originating from the Ru 4*d* states and the localized Cu 3*d* electrons with S = 1/2 spins. Further investigations such as angle-resolved photoemission measurements are needed for understanding the *d*-electron heavy-mass behavior in $SrCu_3Ru_4O_{12}$.

REFERENCES

1. W. Kobayashi, I. Terasaki, J. Takeya, I. Tsukada, and Y. Ando, J. Phys. Rev. Jpn. **73**, 2373 (2004).
2. T.-W. E. Tsang, K. A. Gschneidner, Jr., O. D. McMasters, R. J. Stierman, and S. K. Dhar, Phys. Rev. B **29**, 4185 (1984).
3. T. Sudayama, Y. Wakisaka, K. Takubo, T. Mizokawa, W. Kobayashi, I. Terasaki, S. Tanaka, Y. Maeno, M. Arita, H. Namatame, and M. Taniguchi, Phys. Rev. B **80**, 075113 (2009).
4. H. Liu, Y. Cao, Y. Xu, D. J. Gawryluk, E. Pomjakushina, S.-Y. Gao, P. Dudin, M. Shi, L. Yan, Y.-F. Yang, and H. Ding, Phys. Rev. B **102**, 035111 (2020).
5. H.-P. Xiang, X.-J. Liu, E.-J. Zhao, J. Meng, and Z.-J. Wu, Phys. Rev. B **76**, 155103 (2007).
6. H. Anzai, K. Morikawa, H. Shiono, S.-i. Ideta, K. Tanaka, T. Zhuang, K. T. Matsumoto, and K. Hiraoka, Phys. Rev. B **101**, 235160 (2020).
7. L. H. Tjeng, S.-J. Oh, E.-J. Cho, H.-J. Lin, C. T. Chen, G.-H. Gweon, J.-H. Park, J. W. Allen, T. Suzuki, M. S. Makivic, and D. L. Cox, Phys. Rev. Lett. **71**, 1419 (1993).

Spin- and Angle- Resolved Photoelectron Spectroscopy of Fe_4N Thin Films

K. Nakanishi[a], K. Ohwada[a], K. Kuroda[a,b], K. Sumida[c], H. Sato[d], K. Miyamoto[d], T. Okuda[d], S. Isogami[e], K. Masuda[e], Y. Sakuraba[e,f] and A. Kimura[a,b]

[a]*Graduate School of Advanced Science and Engineering, Hiroshima University, Higashi-Hiroshima 739-8526, Japan*
[b]*International Institute for Sustainability with Knotted Chiral Meta Matter (WPI-SKCM^2), Higashi-Hiroshima 739-8526, Japan*
[c]*Materials Sciences Research Center, Japan Atomic Energy Agency (JAEA), Sayo-cho 679-5148, Japan*
[d]*Hiroshima Synchrotron Radiation Center, Hiroshima University, Higashi-Hiroshima 739-0046, Japan*
[e]*National Institute for Materials Science, Tsukuba 305-0047, Japan*
[f]*PRESTO, Japan Science and Technology Agency, Saitama 332-0012, Japan*

Keywords: Fe_4N Film, Inverse Tunneling Magnetoresistance, Minority spin, Spin- ARPES

Under big concerns about the explosive growth of energy consumption in the information technology, spintronics is regarded as a promising solution. Fe_4N has long been attracting attention for various spintronic applications [1]. This is not only due to the ferromagnetism with Curie temperature of 760 K but also the perfect negative spin-polarization [2]. For example, the magnetic tunnel junctions (MTJs) with Fe_4N electrodes shows an inverse tunneling magnetoresistance (inverse TMR) effect with high (low) electric resistance for parallel (anti-parallel) magnetization configuration in between the magnetic free and pinned layers, and the highest TMR ratio with negative sign has been recorded at both low and ambient temperatures [3,4]. Negative anisotropic magnetoresistance (negative-AMR) in longitudinal [5] and transverse geometries [6,7] has been observed. The inverse-current induced magnetization switching phenomenon [8], and the in-plane anisotropic and relatively large anomalous Nernst conductivity [9] are the promising characteristics for applications. It should be highlighted that these characteristics might be related to the specific electronic band structure of Fe_4N with negative spin polarizaiton originating from the *p-d* hybridization between Fe and N [2]. Therefore, experimental clarification of the bulk band structure of Fe_4N is indispensable to get insight into such electron transport phenomena and to provide an outlook into the development of various functionalities such as spin-torque oscillators [10].

To this end, we have employed a spin- and angle- resolved photoelectron spectroscopy (Spin-ARPES). On the other hand, this technique using conventional light sources in the vacuum ultraviolet region is characterized by high surface sensitivity due to the short mean free path of photoelectrons. Therefore, its application has been limited to materials with cleavage planes, such as layered superconductors and transition metal chalcogenides etc.. For non-layered materials, it has been restricted to elemental crystals in case when their surface cleaning procedures are established. Sputtering and annealing procedures are rarely suitable for multi-element compounds due to element-dependent sputtering rates, which may result in changes in surface stoichiometry. Therefore, the lack of an established surface cleaning procedure is an obstacle to the realization of ARPES on the bulk crystal of Fe_4N. Here, we have chosen a different way to use thin-film samples of Fe_4N grown on MgO substrates and introduced them into the ARPES experimental apparatus without breaking vacuum using an ultra-high vacuum suitcase.

Highly ordered 20-nm-thick γ'-Fe_4N single-crystal films were deposited on MgO(001) substrates at room temperature using a reactive magnetron nitride sputtering technique at National Institute of Materials Science (NIMS). The epitaxial relationship between Fe_4N and MgO was Fe_4N[100](001) ‖ MgO[100](001). An electrode layer of Cr/Ag/Cr was inserted to increase the electrical conductivity between the thin film and the sample holder (see Fig. 1). The film samples were transported from NIMS to the preparation chamber of the spin-ARPES apparatus at HiSOR *via* the vacuum suitcase chamber and were post-annealed at 400°C for 30-60 min in an ultra-high vacuum after being transported from the vacuum suitcase. No nitrogen deficiency

and no other impurities were detected by the Auger electron spectroscopy and the flat (001) surface was ensured by the sharp LEED spots. ARPES and spin-ARPES measurements were performed at BL-7 and BL-9B of HiSOR utilizing synchrotron radiation at incident photon energies of 80-120 eV and 50-119 eV, respectively. Spin-ARPES measurement was performed utilizing the ESPRESSO machine composed of the hemispherical analyzer and the VLEED-type spin detector with *s*- and *p*- polarized undulator radiation. The photoelectron spin polarization (P) was estimated from the measured intensity asymmetry $A = (I^+ - I^-)/(I^+ + I^-)$ with the effective Sherman function ($S_{\mathrm{eff}} = 0.3$) through the relation $P = A/S_{\mathrm{eff}}$, where $I^+(I^-)$ represents the reflected electron intensity at the positively (negatively) magnetized Fe(001)-p(1×1)O target of the spin detector [11,12].

Figure 1(a) shows the ARPES image of Fe_4N thin film in the ΓM direction. We have observed three band dispersions that cross the Fermi level (E_F) at $k_{||}$ = -1.0, -0.5 and +0.5 Å^{-1}. Figure 1(b) shows the spin-resolved energy distribution curves deduced by $I_{\uparrow\downarrow} = 0.5I(1 \pm P)$ at the fixed wavenumber of the red line in Fig. 1(a), where $I_\uparrow$ ($I_\downarrow$) corresponds to the photoelectron intensity in the majority (minority) spin channel and $I = I_\uparrow + I_\downarrow$. We find that $I_\uparrow$ is dominant in the energy (E-E_F) from -1.6 eV to -0.5 eV, while $I_\downarrow$ gradually increases with increasing energy and gets much higher than $I_\uparrow$ in the vicinity of E_F. Such minority-spin dominated features are similarly observed at other wavenumbers.

In summary, the minority-spin dominated character of the band structures in the vicinity of E_F has been unveiled experimentally for Fe_4N thin film. Our finding provides deep insights into the mechanism of the inverse tunneling magnetoresistance effect, the negative anisotropic magnetoresistance, and the enhanced spin pumping in Fe_4N, which will help the development of spintronics devices.

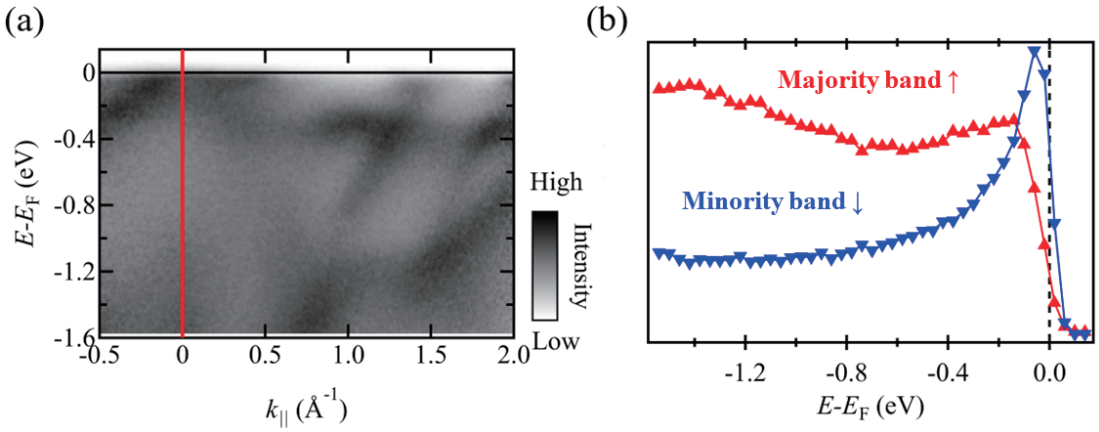

FIGURE 1. (a) ARPES energy dispersions curves along the ΓM line. (b) Spin-resolved energy distribution curves acquired at a wavenumber position denoted with red dashed line in panel (a).

REFERENCES

1. S. Isogami, and Y. K. Takahashi, Adv. Electron. Mater. **9**, 2200515 (2023).
2. S. Kokado, N. Fujiwara, K. Harigaya, H. Shimizu, Phys. Rev. B **73**, 172410 (2006).
3. K. Sunaga, M. Tsunoda, K. Komagaki, Y. Uehara, and M. Takahashi, J. Appl. Phys. **102**, 013917 (2007).
4. Y. Komasaki, M. Tsunoda, S. Isogami, and M. Takahashi, J. Appl. Phys. **105**, 07C928 (2009).
5. M. Tsunoda, H. Takahashi, S. Kokado, Y. Komasaki, A. Sakuma, and M. Takahashi, Appl. Phys. Express **3**, 113003 (2010).
6. K. Kabara, M. Tsunoda, and S. Kokado, AIP Adv. **6**, 055818 (2016).
7. S. Kokado, and M. Tsunoda, J. Phys. Soc. Jpn. **91**, 044701 (2022).
8. S. Isogami, M. Tsunoda, Y. Komasaki, A. Sakuma, and M. Takahashi, Appl. Phys. Express **3**, 103002 (2010).
9. S. Isogami, K. Takanashi, and M. Mizuguchi, Appl. Phys. Express **10**, 073005 (2017).
10. H. Suto, T. Nakatani, Y. Kota, N. Asam, H. Iwasaki, K. Amemiya, T. Mitsui, S. Sakai, S. Li, Y. Sakuraba, J. Magn. Magn. Mater. **557**, 169474 (2022).
11. T. Okuda *et al*. Rev. Sci. Instrum. **82**, 103302 (2011).
12. T. Okuda *et al*., J. Electron Spectrosc. Relat. Phenom. **201**, 23 (2015).